PARTITIONING OF GASES TO ICE IN THE ATMOSPHERE: EFFECTS ON NITRIC ACID AND THE FORMATION OF SULFATE

By

BRIAN P. MARMO

A thesis submitted to the

Graduate School-New Brunswick

Rutgers, The State University of New Jersey

in partial fulfillment of the requirements

for the degree of

Master of Science

Graduate Program in Atmospheric Science

written under the direction of

Dr. Annmarie G. Carlton

and approved by

_____

_____

_____

_____

New Brunswick, New Jersey

JANUARY, 2013

ABSTRACT OF THESIS

PARTITIONING OF GASES TO ICE IN THE ATMOSPHERE: EFFECTS ON NITRIC ACID AND THE FORMATION OF SULFATE

By BRIAN P. MARMO

Thesis Director:
Dr. Annmarie G. Carlton

This thesis describes the first implementation of gas-to-ice partitioning of three inorganic gases (HNO_3, SO_2 and H_2O_2), along with subsequent chemical reactions and changes in gas phase and particle mass concentrations in the Community Multiscale Air Quality (CMAQ) chemical transport model. Adsorbed HNO_3 was assumed to condense and partition to the aerosol phase. Adsorbed SO_2 and H_2O_2 reacted to form sulfate on the ice surface. Four different simulations were performed with CMAQv4.7.1 for August 12^{th}-25^{th} of 2005: 1) base case simulation without the addition of lightning-generated NO_x, 2) a simulation with the addition of lightning-generated NO_x, 3) 100% partitioning case and 4) 25% partitioning case. Simulations 3) and 4) provided an upper and lower bound for the partitioning of adsorbed HNO_3 to remain in the aerosol phase. Considerable decreases, greater than 25% in gas phase HNO_3, were noted in the 100% partitioning case for 200-600 mb, with the largest changes at 300 mb and 400 mb. Potential effects induced on other gases in the nitrogen budget (NO_x and HONO) and oxidant cycling of atmosphere (O_3) due to gas-to-ice partitioning of HNO_3 were

considered. Decreases in NO_x and HONO gas mixing ratios were found to be as high 20%, but were generally less than 10%. Changes in O_3 concentration were less than 1%. Increases in nitrate aerosol mass concentration were as high as 0.15 $\mu g/m^3$ for the upper levels of the atmosphere. No changes in H_2O_2, SO_2, or sulfate aerosol concentrations were observed.

Acknowledgements

I would first like to thank my advisor Dr. Annmarie G. Carlton for all of her guidance and support over the last two years. Whether it was in the classroom or in a research meeting, Dr. Carlton's dedication and enthusiasm towards her students was evident to all. It was an honor to be her first graduate student at Rutgers University. Next, I would like to thank my committee members, Dr. Barbara Turpin, Dr. Mark Miller and Dr. Rob Pinder. Whether it was their assistance in a course in the Atmospheric Science program, or help on my research project, their guidance was essential. I would also like to acknowledge K. Wyat Appel at the EPA, whose work served as a major motivation for this study. Appreciations also go out to the members of the Carlton research group, Caroline Farkas, Khoi Nguyen, Neha Sareen and Partha Bhattacharjee, who provided support in research meetings and the research lab. Other graduate students I would like to acknowledge for help on my project or in my coursework include: Matthew Niznik, Anthony DeAngelis, Michael Erb, Stephen Nicholls, Lalitha Kommajosyula, Jessie Sagona, Ross Alter, Allie Marquardt Collow, Tom Collow, Zhongyu Kuang, Jeffrey Kirkland, Diana Ortiz, Anjuli Ramos, Natasha Hodas, and Ben Kravitz. Others I would like to acknowledge for their assistance include Dr. Virendra Ghate, Michael Ferner, Mina Azer and Kyle Zahn. Lastly, I would like to thank the rest of the Department of Environmental Sciences for two great years.

Table of Contents

List of Tables

List of Illustrations

Introduction

The adsorption of chemical species to ice has been examined in laboratory, modeling and field studies (Clegg and Abbatt, 2001a; Clegg and Abbatt, 2001b; Marécal et al., 2010; Tabazadeh et al., 1999; Popp et al., 2004; Krämer et al., 2008). In this work, the gas-to-ice partitioning of SO_2, H_2O_2 and HNO_3 in the upper levels of the atmosphere is considered using a chemical transport model. SO_2 and H_2O_2 generate interest because of the possible reaction between the two to form sulfate on the surface of the ice (Clegg and Abbatt, 2001b).

Cloud Ice in the Summertime

Summertime cloud ice mixing ratios can be substantial, along with mixing ratios of HNO_3, SO_2, and H_2O_2. Ice crystal concentrations in clouds can be large at around 258 K (Rogers and Yau, 1989). High clouds such as cirrus are typically all ice and deep clouds, typical of summertime convection over North America, contain substantial amounts of ice crystals (Marécal et al., 2010). These deep convective clouds also have the ability to produce lightning. Thus for a study that focused on the chemistry of deep convective clouds, lightning-generated NO_x, based on the work of Allen et al. (2012), was included in the model simulations.

SO_2 and H_2O_2

SO_2 is oxidized in the atmosphere to form sulfate, which contributes to the harmful effects of acid deposition, regional haze and other air quality issues (Appel et al., 2011; Civerolo et al., 2010). An important motivation for this study was the CMAQv4.7

(Community Multiscale Air Quality) model performance of sulfate. Between 2002 and 2006, deposition values of sulfate were only under predicted by CMAQ during the summers of 2002 and 2005 for the eastern United States (Appel, 2010). A study by Civerolo et al. (2010) found that CMAQ had over predicted dry deposition values of SO_2 for 2005. The fact that sulfate, which is predominantly formed in the atmosphere, is underestimated while its precursor (SO_2) is overestimated suggests that the model is missing a loss/formation process (rather than an emission source). It is hypothesized here that the aforementioned reaction between SO_2 and H_2O_2 on ice could possibly explain this discrepancy in CMAQ for the summer of 2005.

Clegg and Abbatt (2001a) studied the uptake of SO_2 and H_2O_2 by ice using a coated-wall flow tube coupled to an electron-impact quadruple mass spectrometer between the temperatures 213 K and 238 K and the partial pressures 10^{-7} Torr and 10^{-4} Torr. Typical partial pressures of H_2O_2 found in the upper atmosphere are approximately 10^{-7} Torr, while typical partial pressures of SO_2 are near 10^{-8} Torr. In their study, the uptake of H_2O_2 increased linearly with partial pressure, and was insensitive to surface acidity and temperature. SO_2 partitioning increased with increasing partial pressure and temperature, while the uptake decreased with increasing surface acidity. Uptake by ice of both H_2O_2 and SO_2 was fully reversible in the absence of the other. They also studied SO_2 uptake in the presence of H_2O_2 (Clegg and Abbatt, 2001b). In this experiment, H_2O_2 flow over the ice was sufficient to attain equilibrium between the condensed phase (ice surface) and the gas phase. Uptake of SO_2 was enhanced by the presence of adsorbed H_2O_2 on the ice. This suggests that a reaction between SO_2 and H_2O_2 occurred on the ice surface. Other laboratory studies also concluded that the presence of H_2O_2 increases the

uptake of SO_2 onto ice (Mitra et al., 1990; Conklin et al., 1993; Chu et al., 2000). SO_2 oxidation by H_2O_2 to form sulfate is consistent with the observed enhanced uptake (Chu et al., 2000; Clegg and Abbatt, 2001b). Clegg and Abbatt proposed that this reaction on the surface of the ice was comparable to the oxidation of SO_2 by H_2O_2 in an aqueous solution, as shown below (Clegg and Abbatt, 2001b).

$$H_2O_{2\,(g)} \leftrightarrow H_2O_{2\,(ads)} \quad (1)$$

$$SO_{2\,(g)} \leftrightarrow SO_{2\,(ads)} \quad (2)$$

$$SO_{2\,(ads)} + H_2O \leftrightarrow H^+_{(ads)} + HSO^-_{3\,(ads)} \quad (3)$$

$$HSO^-_{3\,(ads)} + H_2O_{2\,(ads)} \rightarrow HOOSO^-_{2\,(ads)} + H_2O \quad (4)$$

$$HOOSO^-_{2\,(ads)} + H^+_{(ads)} \rightarrow 2H^+_{(ads)} + SO^{2-}_{4\,(ads)} \quad (5)$$

The subscripts (g) and (ads) denote the gas phase and adsorbed phase respectively. Reaction 4 above is the slowest and considered the rate-determining step. Therefore, the rate of the overall reaction (s^{-1}) of SO_2 with H_2O_2 on the surface of the ice is:

$$Rate = k_4\left[HSO^-_3(ads)\right][H_2O_2(ads)] \quad (6)$$

where k_4 (M^{-2} s^{-1}) is the rate constant for Reaction (4), $[HSO^{3-}(ads)]$ is proportional to the amount of gas phase SO_2 that has adsorbed to ice (M), and $[H_2O_2(ads)]$ is the amount of gas phase H_2O_2 that has adsorbed to ice (M). The reaction rate constant for the fourth reaction is shown in Equation 7 (Ervens et al., 2004):

$$k_4 = 7.2 \times 10^7 * EXP\left(-\frac{4000}{T}\right) \quad (7)$$

where T is temperature in Kelvin.

HNO_3

HNO_3 is "sticky" in nature, (Finlayson-Pitts and Pitts, 2000) and has the ability to readily adsorb to surfaces such as ice. HNO_3 also has an important influence on the nitrogen budget (Tabazadeh et al., 1999). For instance, gas phase HNO_3 reactions are a pathway to NO_x formation (Reaction 8-11), a critical factor in ozone formation. In the upper troposphere, ozone is an important greenhouse gas that affects climate through warming. Thus, reductions in HNO_3 and NO_x could generate a negative feedback to climate warming (Popp et al., 2004; Tabazadeh et al., 1999). The upper troposphere O_3/HNO_3 cycle is shown in the reactions below:

$$HNO_3 + hv \rightarrow OH + NO_2 \quad (8)$$

$$NO + O_3 \rightarrow NO_2 + O_2 \quad (9)$$

$$NO_2 + hv \rightarrow NO + O \quad (10)$$

$$O + O_2 + M \leftrightarrow O_3 + M \quad (11)$$

Applying an equilibrium-based approach, Marécal et al. (2010) modeled the uptake of common atmospheric gases by simulated ice particles in convective clouds. The authors found that for a given gas mixing ratio, HNO_3 had the highest potential for uptake by cloud ice due to its largest surface partition coefficient. For example, 85% of

HNO_3 partitioned to ice in the convective clouds on average, while at times, over 98% of HNO_3 adsorbed to ice.

Several field and modeling studies have indicated a strong potential for gas phase HNO_3 to be redistributed by clouds in the upper troposphere (Popp et al., 2004; Krämer et al., 2008; Abbatt, 1997; Tabazadeh et al., 1999; Clegg and Abbatt, 2001a). Popp et al. (2004) measured gas phase and condensed phase HNO_3 from the NASA WB-57F aircraft using the NOAA Chemical Ionization Mass Spectrometer (CIMS) in cirrus clouds over the Florida area. Temperature observations ranged from 197 K to 224 K with pressure values between 122 mb and 224 mb. On average, approximately 16% of HNO_3 in cirrus clouds was found to be in the condensed phase. For some cases, 100% of HNO_3 was in the condensed phase.

Krämer et al. (2008) observed values of cirrus ice water content and molar ratios of HNO_3/H_2O_2 in cirrus clouds to determine the amount of HNO_3 that partitioned to ice. Temperatures ranged between 185 K and 240 K. They found that anywhere from .01% to 100% of HNO_3 adsorbed to cirrus clouds. The highest amount of uptake occurred for tropical cirrus clouds when temperatures were between 190 K and 210 K.

There is currently disagreement in the literature over the reversibility of HNO_3 ice partitioning. Popp et al. (2004) commented that it is difficult to determine the portion of HNO_3 that remained in the gas phase after adsorption. Marécal et al. (2010) described HNO_3 uptake as reversible and a modeling study by Tabazadeh et al. (1999) is supportive, suggesting less than 30% of gas phase HNO_3 is irreversibly removed by cirrus clouds. However in a lab study, Abbatt (1997) concluded that only 20-25% desorbed, suggesting that HNO_3 partitioning is mostly irreversible. Clegg and Abbatt

(2001a) also reported that only a small portion of HNO_3 desorbed from the ice. If large amounts of gas phase HNO_3 condense on the surface of the ice and remain condensed, mass concentrations of aerosol nitrate in the atmosphere could be increased. Thus the adsorption of gas phase HNO_3 to ice could prove to be an important process for climate, long-range pollution transport and air quality.

Methods

Partitioning Gases to Ice

The partitioning to ice framework implemented in this work follows the Langmuir approach as described by Marécal et al. (2010). The number of molecules of a particular gas that will adsorb to the ice surface is directly proportional to the concentration of the gas in the atmosphere, the total surface area of the ice particles and an intrinsic partitioning coefficient of the gas empirically derived from laboratory experiments. Gas-to-ice partition coefficients are typically inversely proportional to temperature. The amount of a gas that adsorbs to the ice surface can be defined by Equation 12 (Marécal et al., 2010):

$$n_s = AK_{linC}n_g \tag{12}$$

where n_s is the gas concentration on the surface of the ice (molecules m^{-3} per air), A is the total surface area of the ice (m^2 m^{-3}), K_{linC} is the partition coefficient (m), and n_g is the gas concentration (molecules m^{-3} per air). The temperature dependence of K_{linC} can be expressed as:

$$K_{linC} = A_p \exp\left(\frac{B_p}{T}\right) \tag{13}$$

where A_p and B_p are parameters that depend on the species and T is temperature in Kelvin (Marécal et al., 2010). For each gas specie there is a range of temperatures for which the adsorption to ice has been determined. Table 1 contains empirical values of the

parameters A_p (m) and B_p (K), and the temperature ranges for which they were determined. These values indicate that for a given gas mixing ratio, HNO_3 partitions with the greatest efficiency for most temperatures.

Table 1 – Values for the parameters A_p and B_p used to determine the partition coefficient for gases HNO_3, SO_2 and H_2O_2. Also included are the temperature ranges. Values for HNO_3 and H_2O_2 are from Marécal et al (2010). The values for SO_2 are from Carver et al. (1999).

Species	A_p (m)	B_p (K^{-1})	Temperature Range (K)
HNO_3	7.5×10^{-7}	4585	214 – 240
SO_2	7.3×10^{-6}	2065	190 – 250
H_2O_2	2.1×10^{-7}	3800	203 – 233

The partition coefficient for H_2O_2 from Marécal et al. (2010) used updated A_p and B_p values from Pouvesle et al. (2010), who found that the uptake of H_2O_2 by ice was more than two orders of magnitude larger than that found in Clegg and Abbatt (2001a). Pouvesle et al. (2010) also found that as temperatures decreased, the adsorption of H_2O_2 increased.

Parameterization of Ice

Ice mixing ratio values from The 5th Generation Mesoscale Model (MM5) Version 3.7.4 were processed with the Meteorology-Chemistry Interface Processor (MCIP) and imported to CMAQ (Appel et al., 2011). Equation 12 describes the total amount of a gas that will partition to the surface of the ice as a surface area limited process. The total ice surface area for the bulk volume of the total cloud ice was calculated from MM5 predicted ice volume mixing ratios (Q_{ice}) with Equations 14 and

15. A non-trivial assumption in this approach is that all ice particles were assumed to be spheres. This assumption represents a lower limit because spheres have the lowest surface area to volume ratio compared to typical ice crystal shapes such as needles, hexagonal plates, columns and dendrites.

$$Q_{ice} = \frac{4}{3}\pi r_e^3 \times \frac{\rho_{ice}}{\rho_{air}} \times N \quad (14)$$

$$SA_{ice} = 4\pi r_e^2 \times N \quad (15)$$

Where Q_{ice} is the ice mixing ratio (kg_{ice}/kg_{air}), r_e is the effective ice radius (m), ρ_{ice} is the density of ice (kg_{ice} m^{-3}), ρ_{air} is the density of air (kg_{air} m^{-3}), and N is the number concentration of ice crystals (m^{-3}). To determine the total ice surface area, the ice effective radius from Ivanova et al. (2001) was used. The ice effective radius is expressed in Equation 16:

$$r_e = \frac{(75.3+0.5895 \times T)}{2} \quad (16)$$

where r_e is the ice effective radius (m) and T is the temperature in Celsius. Using the ice effective radius, the ice mixing ratio and other modeled variables, the total ice surface area was calculated.

Popp et al. (2004) found values for ice surface area from a field study in Florida to be between 2 x 10^2 μm^2 cm^{-3} (2 x 10^{-4} m^2 m^{-3}) and 4 x 10^4 μm^2 cm^{-3} (4 x 10^{-2} m^2 m^{-3}). Clegg and Abbatt (2001b) reported values between 2 x 10^{-7} cm^2 cm^{-3} (2 x 10^{-5} m^2 m^{-3})

for cirrus clouds and 2 x 10^{-4} cm^2cm^{-3} (2 x 10^{-2} m^2 m^{-3}) for convective clouds. When applied to MM5 output, the values for the total ice surface areas using the equations above generally fell within these bounds. Surface areas very rarely were greater than 1 x 10^{-2} m^2 m^{-3}.

Choosing a Time Period

As a result of large discrepancies between CMAQ predicted sulfate and measured sulfate for August 2005 (Appel, 2010) and substantial cloud ice concentrations, it was decided that the two week period of August 12th through August 25th would be studied. Based on calculated spatial averages and the screening of ice mixing ratio for the time period, it was determined that the analysis would focus on the pressure levels that had large ice mixing ratios: 200 mb, 300 mb and 400 mb. In addition, 100 mb, 500 mb and 600 mb had moderate mixing ratios and were also studied. A typical diurnal trend observed in the model for this two weeks was that ice mixing ratios peaked in the afternoon hours (18 UTC to 23 UTC) and evening hours (0 UTC to 8 UTC). These times coincide with when convection is more likely to occur in the summertime. The morning and early afternoon hours (9 UTC to 17 UTC) usually had lower ice mixing ratios.

CMAQ Configuration and Input data

The CMAQ simulations were conducted with inputs as described in detail by Appel et al. (2011). Briefly, output from the MM5 version 3.7.4, nudged with re-analysis data, was processed by MCIP to generate "offline" meteorology fields, including the prediction of cloud ice mixing ratios. Also the AERO5 aerosol module and the Carbon

Bond 05 chemical mechanism with chlorine chemistry extensions were used. Version 3 of the 2002 National Emissions Inventory (NEI) was used to generate non-EGU (electrical generating unit) point sources. Mobile emissions were added using the MOBILE6 model, and satellites were used to make estimates from fire emissions. The emissions inputs were prepared for CMAQ using the Sparse Matrix Operator Kernel Emissions (SMOKE) model.

Substantial SO_2 emissions come from electric utility plants, located primarily in the eastern U.S. (Appel et al., 2011; Civerolo et al., 2010). Gas phase SO_2 is oxidized by OH to form sulfate, while aqueous phase SO_2 is oxidized by either H_2O_2 or O_3 to result in sulfate in the atmosphere (Jacob, 1999). Gas phase HNO_3 is formed from the oxidation of NO_x compounds by OH (Jacob, 1999). Once in the atmosphere, these chemical species are subject to transport by vertical and horizontal advection and removal due to wet and dry deposition.

Gas phase HNO3 can be formed aloft, at the level of cloud ice, from the oxidation of NO_x compounds. Deep convective clouds that have substantial amounts of ice are also likely to have lightning and produce lightning-generated NO_x. For this reason, lightning-generated NO_x parameterizations were added to the CMAQ code, based on the work of Allen et al. (2012). The addition of lightning-NO_x production greatly increases upper troposphere NO_x concentrations (Allen et al., 2012). CMAQ determined the amount of lightning-produced NO by using convective precipitation rates from the MM5 model output (Appel et al., 2011). Observed flashes by the National Lightning Detection Network (NLDN) were also used with the climatological ratio of intra-cloud flashes to

cloud-to-ground flashes (IC/GC) determined in Boccippio et al. (2001). This method also assumes that 500 moles of NO were generated for each flash of lightning.

The implementation of lightning-NO_x production in CMAQv4.7.1 required the addition of the CMAQ subroutine LTNG_DEFN.F. This subroutine was very similar to the one found in CMAQv5.0, with slight differences in the syntax. A lightning-NO_x parameter file was prepared using NLDN monthly flash totals, the climatological ratio of intra-cloud to cloud-to-ground flashes and convective precipitation rates. Additions to the CMAQ subroutine EMIS_DEFN.F were also necessary to calculate the in-line lightning-generated NO_x.

Simulations

CMAQ simulations were conducted with 12 km by 12 km grid cells (240 rows by 279 columns) horizontal resolution for the eastern two-thirds of the U.S., including southern Canada and northern Mexico (Appel et al., 2011). The simulations were performed for 24 vertical layers for August 10^{th}-25^{th}, 2005 (total of 1,607,040 computational cells). The first two days are excluded from this analysis to allow for model "spin up".

A summary of the four simulations performed for this work can be seen in Table 2. The first simulation was performed with no additions or changes made to the CMAQ code. This run will be referred to as the base case. The second simulation was conducted with only the addition of lightning NO_x. This run will be referred to as the LNO_x case.

Two additional sensitivity simulations were performed for HNO_3 partitioning to ice. Due to uncertainty in the literature on the reversibility of HNO_3 partitioning, two

bounding simulations were conducted. Both sensitivity simulations included lightning NO_x. For each simulation, gas phase HNO_3 partitioned to ice, based on Equation 12. In the third simulation, the 100% partitioning case, all gas phase HNO_3 that adsorbed to the ice partitioned to the aerosol phase, and it was assumed that all the adsorbed HNO_3 remained condensed. For the last simulation, the 25% partitioning case, 25% of the gas phase HNO_3 that adsorbed to the ice partitioned and remained in the condensed phase. These runs serve as the upper and lower bound for the amount of gas phase HNO_3 that partitions to and remains in the condensed phase while at cloud level. The amount that partitioned to the condensed phase was subtracted from the gas phase concentration. The 100% partitioning case is comparable to the studies that found adsorbed HNO_3 to be mostly irreversible (Abbatt, 1997; Clegg and Abbatt, 2001a), while the 25% partitioning case is comparable to the studies that found adsorbed HNO_3 to be largely reversible (Marécal et al., 2010; Tabazadeh et al., 1999). Eventually, any HNO_3 that adsorbed to the ice in either simulation could partition back into the gas phase during subsequent calculations during operator splitting, in particular during the re-establishment of chemical equilibrium for inorganic species between the gas and aerosol phase.

Also included in the last two simulations was the gas-to-ice partitioning and subsequent reaction of SO_2 and H_2O_2 to form sulfate on ice particles. SO_2 and H_2O_2 partitioned according to Equation 12 and reacted according to Equation 6. Unreacted SO_2 and H_2O_2 desorbed back into the gas phase. Reacted SO_2 and H_2O_2 were subtracted from the gas phase concentration for each gas respectively, and formed sulfate was added to accumulation mode sulfate aerosol mass. All ice partitioning code was added to the

CMAQ subroutine cldproc_acm.F (see Appendix B). An overview of the processes at work in this study can be seen in Figure 1.

Table 2 – The four major simulations performed for this work.

Run Name	Inclusion of LNO_x	Partitioning of HNO_3 to Ice	Amount of Adsorbed HNO_3 Partitioned to Aerosol Phase	Reaction of SO_2 and H_2O_2 on Ice
Base Case	NO	NO	NONE	NO
LNO_x Case	YES	NO	NONE	NO
100% Partitioning Case	YES	YES	100 %	YES
25% Partitioning Case	YES	YES	25 %	YES

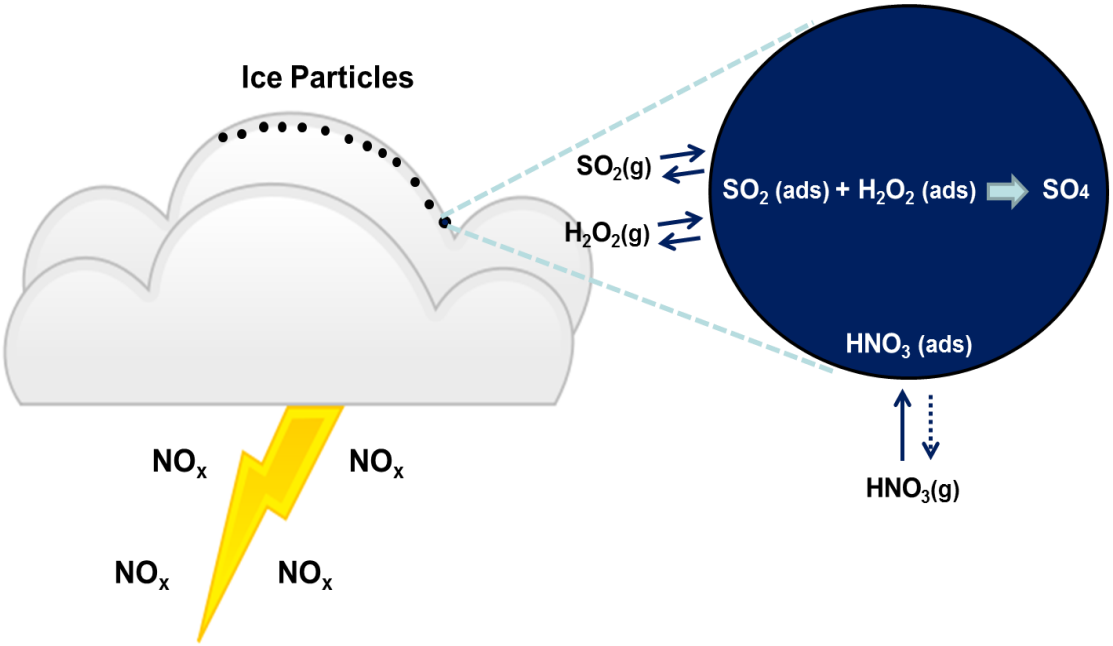

Figure 1 – An overview of the processes at work in this study. Gas phase SO_2 and H_2O_2 adsorb to the ice and react to form sulfate. Unreacted SO_2 and H_2O_2 desorb back to the gas phase. Gas phase HNO_3 partitions to the ice, but since its reversibility is uncertain, two sensitivity studies were performed. Lightning-generated NO_x was included because of its influence on gas phase HNO_3 concentrations.

Comparison to Observed Measurements

To assess CMAQ's predictive ability for species studied in this work, a comparison for particulate nitrate mass concentration was made comparing the LNO_x case predictions to measurements made at monitoring sites. The IMPROVE (Interagency Monitoring of PROtected Visual Environments) network is a collection of monitoring sites located in rural regions across the U.S. The measurements made at the IMPROVE sites were compared to corresponding predictions grid cells in CMAQ. The IMPROVE network was chosen because it contained more available observations for the modeled period than other monitoring networks. Also, since these measurements were made in rural locations, the observations were less likely to be influenced by localized pollution sources found in urban settings.

Results

Model Performance

CMAQ performed relatively well on the days where detailed measurements of particulate nitrate mass concentration were made (see Appendix A, Figure S-1). A small normalized mean bias of 1.03% was found between CMAQ predictions and the IMPROVE measurements. A fairly large over prediction by the CMAQ was seen for August 17th. On the other four days, the model either slightly overestimated or underestimated, indicating there was not a systematic bias in one direction.

The Addition of Lightning NO_x

Results from the LNO_x case were compared to the base case. Figure 2a displays a vertical cross section of the difference in NO_2 concentration between the LNO_x case and the base case at 33°N with pressures ranging from 1000 mb to 100 mb. The figure is for 17Z on Aug 14th. Long bands of increases in gas phase mixing ratios of NO_2 with peaks of approximately 2 ppb were located from 300 mb to 800 mb between 105°W and 100°W, and also near 80°W. While for a different region and time period, Figure 13 of Allen et al. (2012) shows a similar vertical pattern, with episodic peak increases in NO_2 of up to 1 ppb. Figure 2b represents the difference in gas phase HNO_3 concentration between the LNO_x case and base case for the same latitude and time period as Figure 2a. In this figure, a region of increases in gas phase HNO_3 near 80°W corresponds in space and time with the band of increases in NO_2 found in Figure 2a.

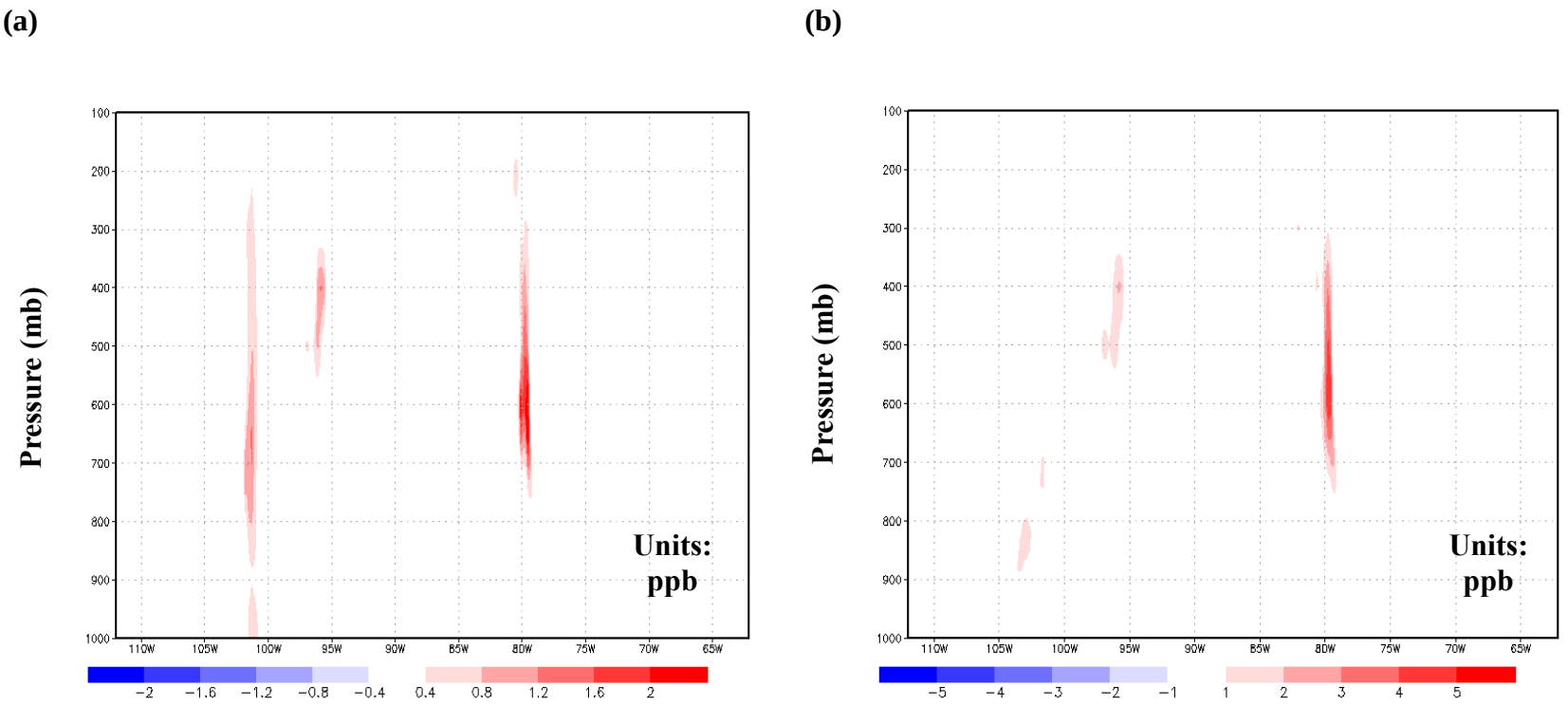

Figure 2a – Vertical cross section of absolute difference in NO_2 concentration (ppb) between LNO_x case and base case from 1000 mb to 100 mb for latitude of 33°N. Figure is for 17Z on August 14th. A similar pattern in the vertical can be seen in Figure 13 of Allen et al. (2012). While this figure and Figure 13 of Allen et al. (2012) are for two different time periods and two different regions, differences in NO_2 concentrations between the LNO_x case and base case are apparent in both figures.

Figure 2b – Vertical cross section of absolute difference in gas phase HNO_3 concentration (ppb) between LNO_x case and base case from 1000 mb to 100 mb at latitude of 33°N for 17Z on August 14th.

Changes in Gas Phase HNO_3

Changes in HNO_3 gas phase mixing ratios of over 25% were seen in various regions for several pressure levels throughout the 14 day time period when comparing the LNO_x case to the ice partitioning cases. Decreases in HNO_3 gas phase concentrations were located in regions where ice particles and HNO_3 were co-located in space and time. Figures 3a and 3b show the ice mixing ratio and the LNO_x case gas phase HNO_3 concentration respectively for 0Z on August 12 at 400 mb.

Figure 4a shows the absolute difference in gas phase HNO_3 between the 100% partitioning case and the LNO_x case, while Figure 4b displays the difference as a percent change in gas phase HNO_3 for the same time and pressure level as Figures 3a and 3b. Absolute decreases in gas phase HNO_3 due to partitioning to ice ranged from 0 to >0.10 ppb. The largest decreases were seen in northern and western Texas, where decreases were greater than 0.10 ppb. Other regions with noticeable decreases were observed in western Kentucky and southern Indiana, where decreases were near 0.06 and 0.08 ppb respectively. Regions such as western Kentucky had percent decreases in gas phase HNO_3 concentrations of over 25%. Fairly large percent decreases were still witnessed in regions of western and northern Texas. It is interesting to note that the areas of greatest absolute decrease did not necessarily coincide with the areas of greatest percent decrease. A key insight for this time and throughout the 14 day period is that the regions of largest HNO_3 concentration change required the temporal and spatial co-location of both gas phase HNO_3 and cloud ice, but were not necessarily located where either of them was at a maximum.

In Figures 4a and 4b, regions of large (gas phase) HNO_3 differences of alternating sign are seen over the northern part of the domain. These alternating patterns are not differences in concentration caused by numerical noise. When comparing multiple model runs of the 100% partitioning case, very little, if any numerical noise was seen (see Appendix A, Figure S-2). Thus, these alternating regions of large HNO_3 differences are more likely caused by actual changes in predicted HNO_3 concentrations. Even though gas phase HNO_3 partitions to the aerosol phase, some fraction will eventually partition back to the gas phase to re-establish chemical equilibrium during other processes in CMAQ. For example, gas phase HNO_3 will adsorb to the ice during the cloud processing science process (cldproc_acm.F). During the chemistry science process, the chemical equilibrium is calculated and re-established (isrpia.inc). This partitioning back and forth between the two phases may contribute to this alternating pattern.

This region of alternating patterns is also spatially similar to where the jet stream (fastest winds) is located. Figure S-3a (see Appendix A) displays wind speeds in m/s, while Figure S-3b (see Appendix A) shows the absolute difference in gas phase HNO_3 between the 100% partitioning case and the LNO_x case. Both plots are for 0Z on August 12^{th} at 300 mb. Large wind speeds are located in the northern central U.S. and Maine (Figure S-3a). These regions correspond to where large alternating patterns of gas phase HNO_3 differences are located (Figure S-3b). Therefore, it may be more difficult to numerically re-establish equilibrium of gas phase HNO_3 in CMAQ when wind speeds are faster.

(a) **(b)**

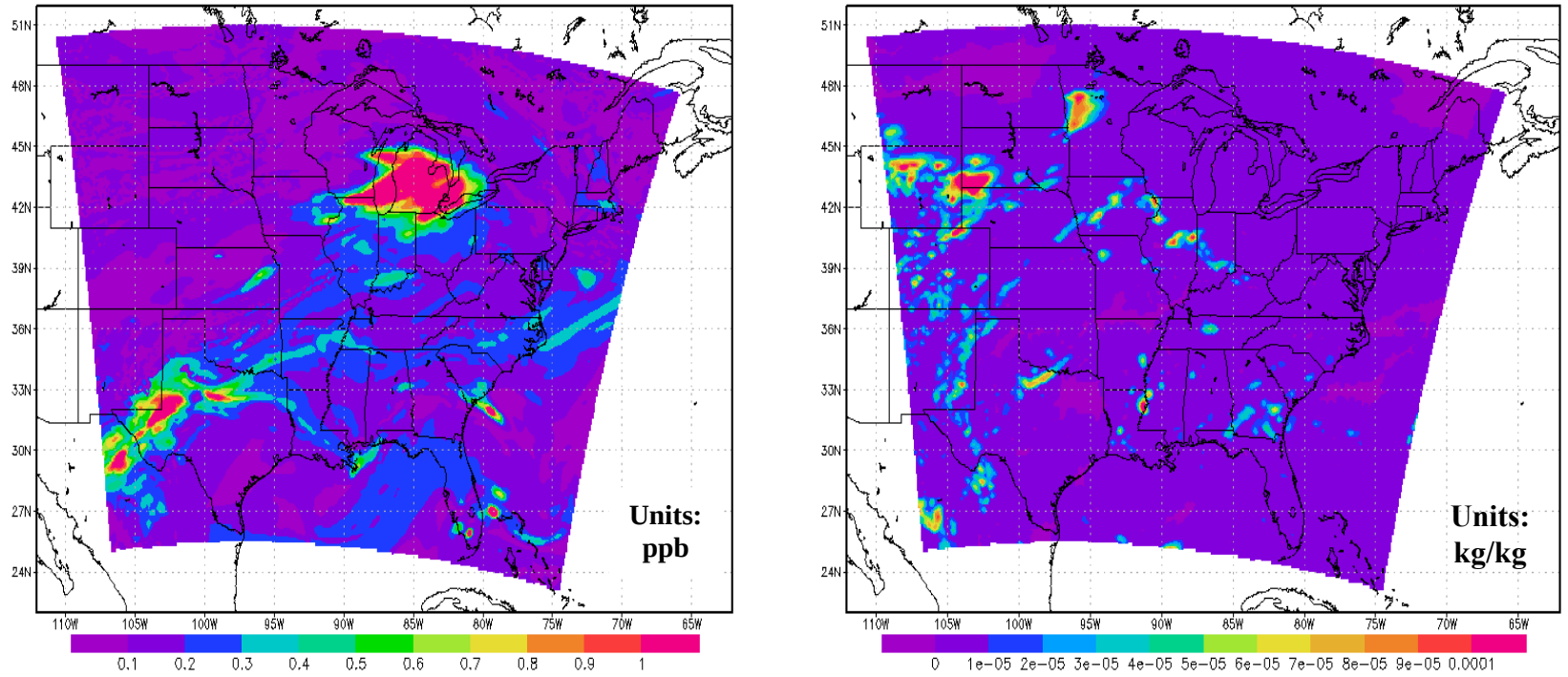

Figure 3a – Gas phase HNO_3 concentration (ppb) for LNO_x case at 400 mb for 0Z on August 12th.

Figure 3b – Ice mixing ratio (kg/kg) at 400 mb for 0Z on August 12th. Peaks in gas phase HNO_3 and cloud ice were not co-located spatially or temporally at this time or for the majority of the two week time period.

(a) **(b)**

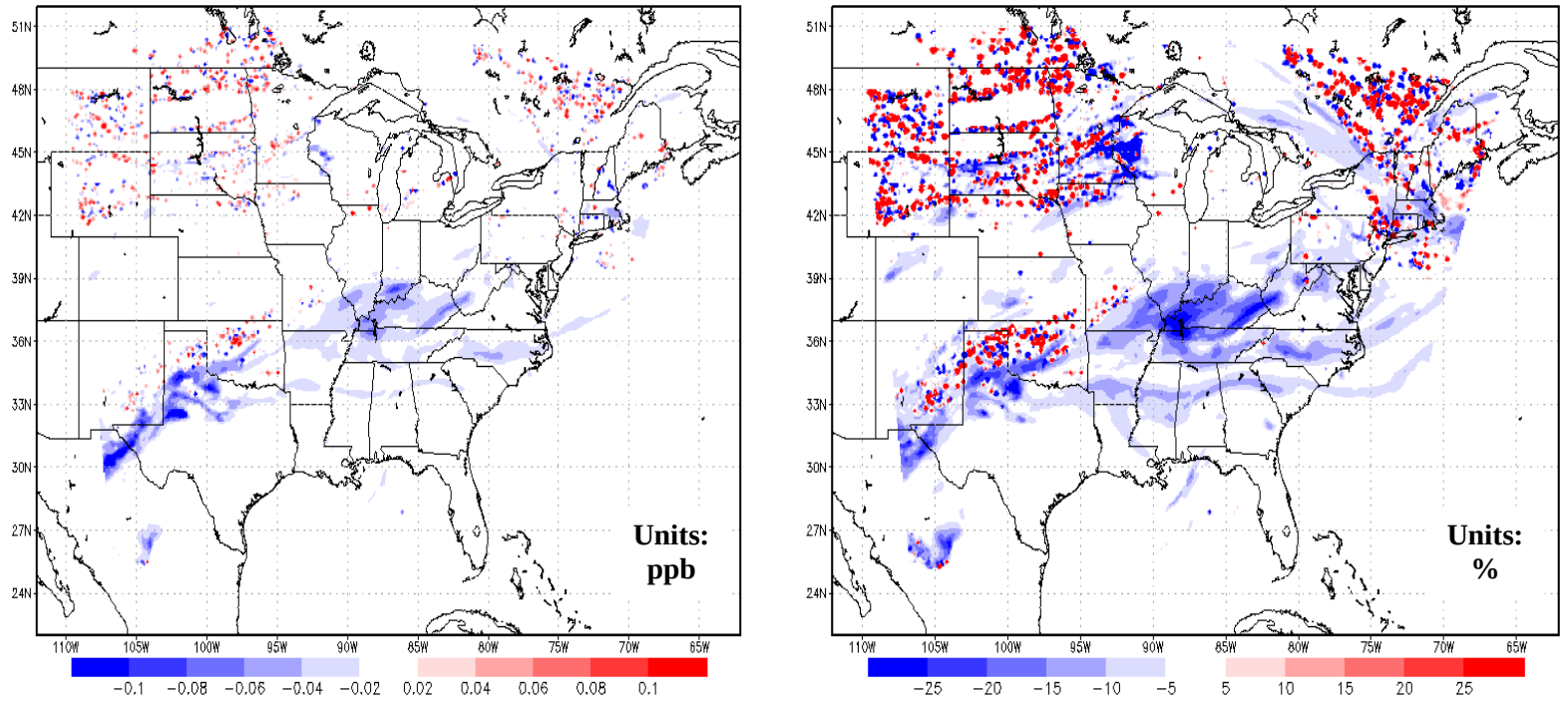

Figure 4 – Absolute differences (ppb) (a) and percent differences (b) in gas phase HNO_3 concentration between 100% partitioning case and LNO_x case at 400 mb for 0Z on August 12th. Large differences in gas phase HNO_3 were often located at 400 mb.

For the 25% partitioning case, decreases in gas phase HNO_3 concentrations showed a similar spatial pattern to the 100% partitioning case in absolute differences (Figure 5a) and in percent differences (Figure 5b). The decreases in gas phase HNO_3 concentration ranged from 0 ppb to >0.10 ppb. Smaller differences were witnessed over regions of Kentucky, southern Indiana and northern Texas, and decreases greater than 0.10 ppb can be seen over northern Mexico. Over western Kentucky, percent decreases in gas phase HNO_3 concentrations of near 25% were observed. Overall, the spatial extent and magnitude of the absolute and percent differences were slightly smaller than in the 100% partitioning case. As seen in Figures 4a and 4b, regions of large (gas phase) HNO_3 differences of alternating sign were also present over the northern part of the domain in Figures 5a and 5b.

The greatest differences in gas phase HNO_3 concentration for an individual time step were frequently at 300 or 400 mb (Figures 4 and 5), but changes also occurred at 200 mb, 500 mb, 600 mb and 650 mb. Figure 6a represents a vertical cross section at 33°N from 1000 mb to 100 mb displaying absolute differences in gas phase HNO_3 between the 100% partitioning case and the LNO_x case for 10Z on August 23. A sizeable region of decreases in gas phase HNO_3 of over 0.1 ppb, with peak decreases of around 0.24 ppb, was present ranging from 300 mb to 600 mb between 90°W and 85°W (which corresponds to northern Alabama). Decreases in gas phase HNO_3 of between 0.06 ppb and 0.10 ppb were witnessed between 110°W and 100°W (southern New Mexico and near panhandle region of Texas) from 300 mb to 700 mb.

(a) **(b)**

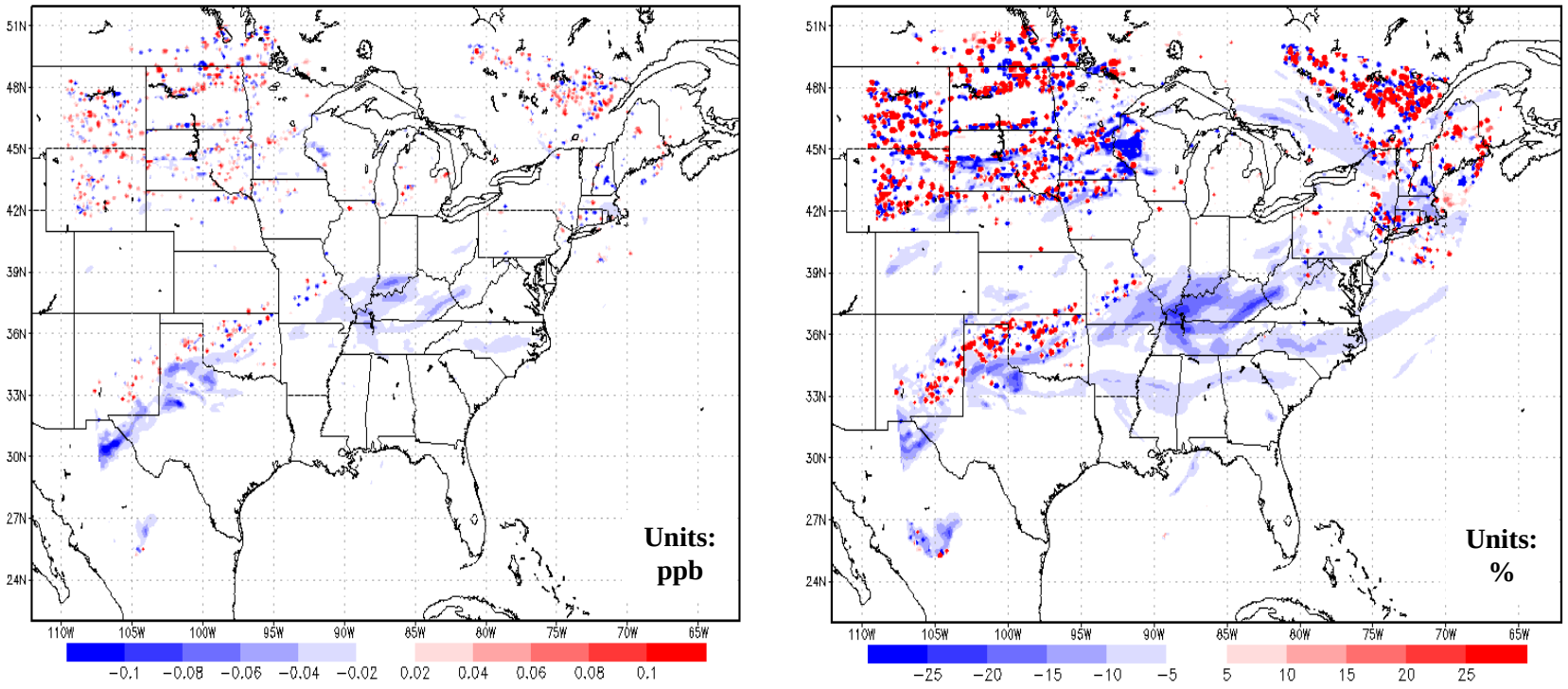

Figure 5 – Absolute differences (ppb) (a) and percent differences (b) in gas phase HNO_3 concentration between 25% partitioning case and LNO_x case at 400 mb for 0Z on August 12th. The spatial extent and magnitude of the absolute and percent differences were slightly smaller than in the 100% partitioning case (Figures 4a and 4b).

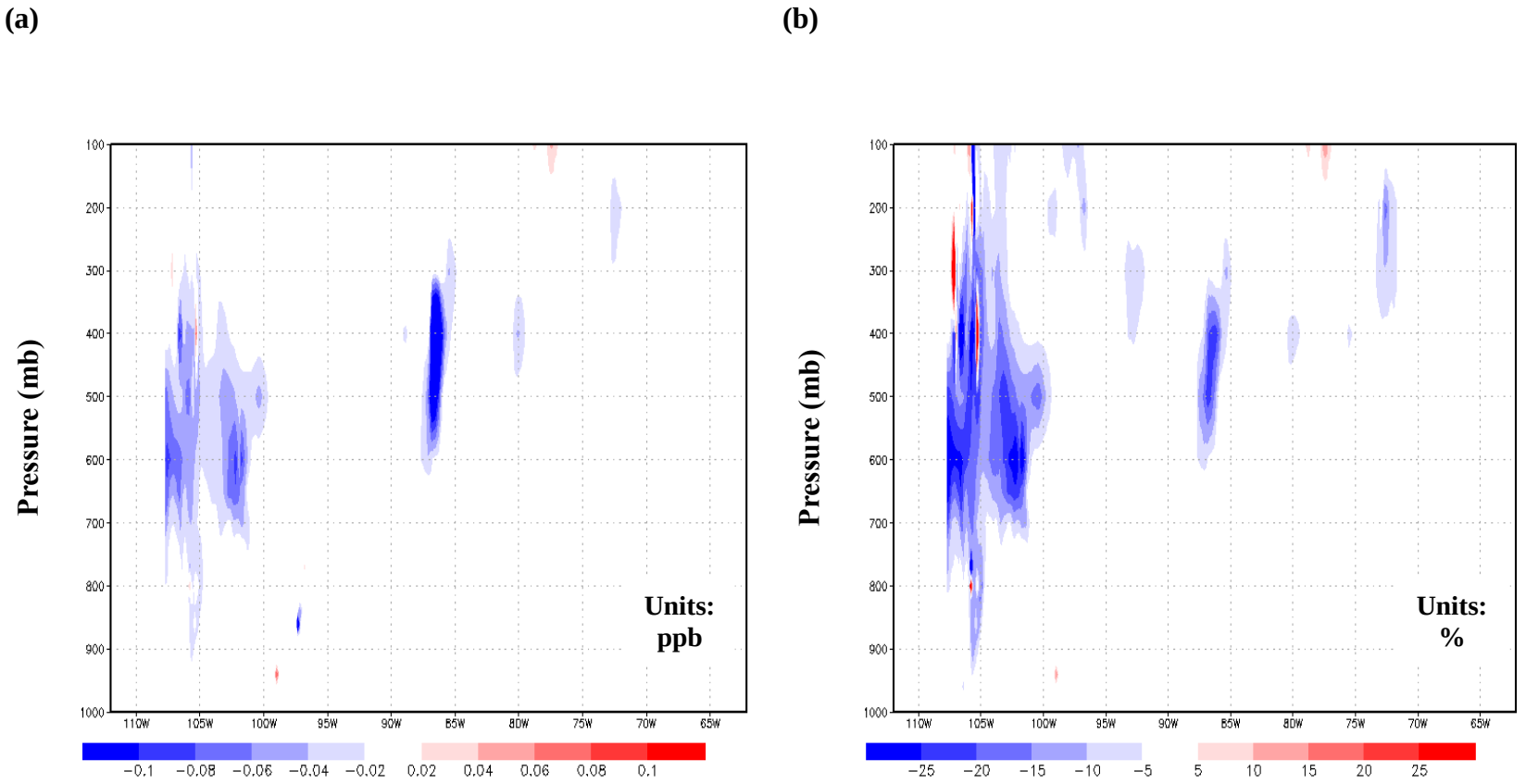

Figure 6 – Vertical cross section of absolute differences (ppb) (a) and percent differences (b) in gas phase HNO_3 concentration between 100% partitioning case and LNO_x case from 1000 mb to 100 mb at 33°N for 10Z on August 23rd. Large decreases were not only present at 400 mb, but also occurred at 300 mb, 500 mb, 600 mb and 650 mb.

The percent differences in gas phase HNO_3 concentration for the same time and latitude followed a similar spatial distribution (Figure 6b). Considerable areas of percent decreases in gas phase HNO_3 of over 25% were present in the western regions of the domain around 600 mb. It is interesting to note that the regions of largest decreases in gas phase HNO_3 were not spatially similar to the areas of largest ice mixing ratios (Figure 7), or gas phase HNO_3.

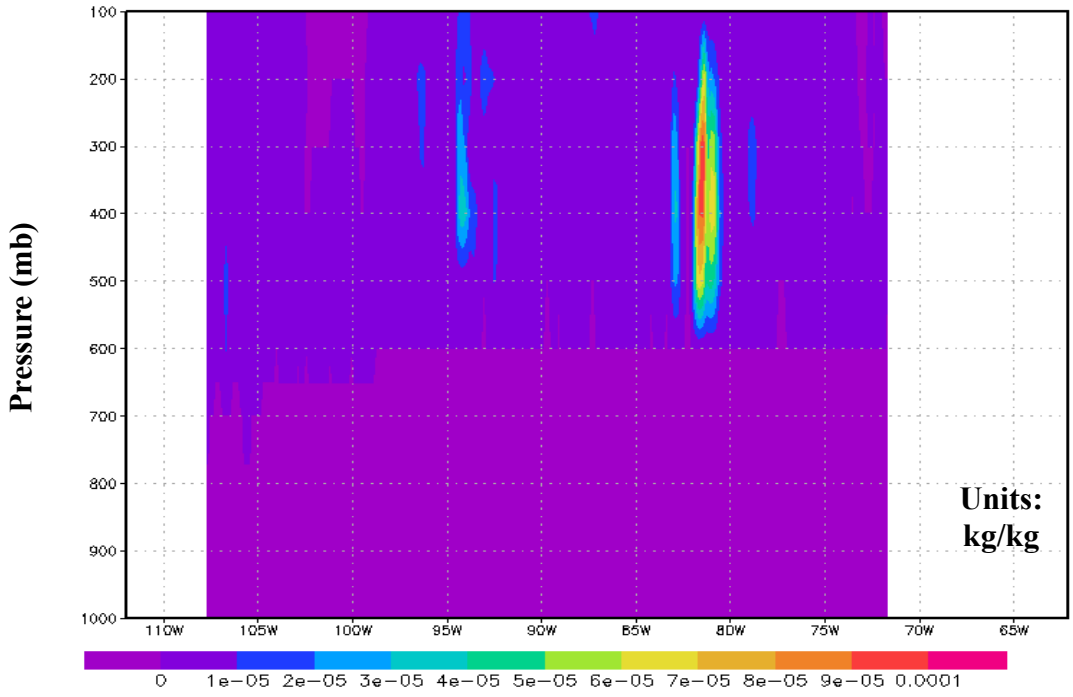

Figure 7 – Vertical cross section of ice mixing ratio (kg/kg) from 1000 mb to 100 mb at 33°N for 10Z on August 23rd. The largest ice mixing ratios did not correspond spatially with the largest decreases in gas phase HNO_3.

For the 25% partitioning case, absolute decreases (Figure 8a) in the gas phase HNO_3 concentration were smaller than the 100% partitioning case (Figure 6a). The region from 300 mb to 600 mb between 90°W and 85°W had decreases in gas phase HNO_3 concentration of over 0.1 ppb, but the peak decrease was around 0.18 ppb. Even though only twenty five percent of adsorbed HNO_3 was removed from the gas phase and remained condensed, the 25% partitioning case was fairly similar in spatial extent and magnitude to the 100% partitioning case. The same was true for the percent differences in gas phase HNO_3, where decreases between 15% and 25% were still widespread (Figure 8b).

Figure 9a shows the absolute difference and Figure 9b shows the percent difference in gas phase HNO_3 concentration between the 25% partitioning case and 100% partitioning case. Both figures are vertical cross sections between 1000 mb and 100 mb at 33°N for 10Z on August 23th. Figure 9a shows peak differences in gas phase HNO_3 of approximately 0.08 ppb around 400 mb between 90°W and 85°W. Figure 9b displays peak percent differences of over 25% near the 105°W longitude line. However, most of the domain had percent differences of less than 25%.

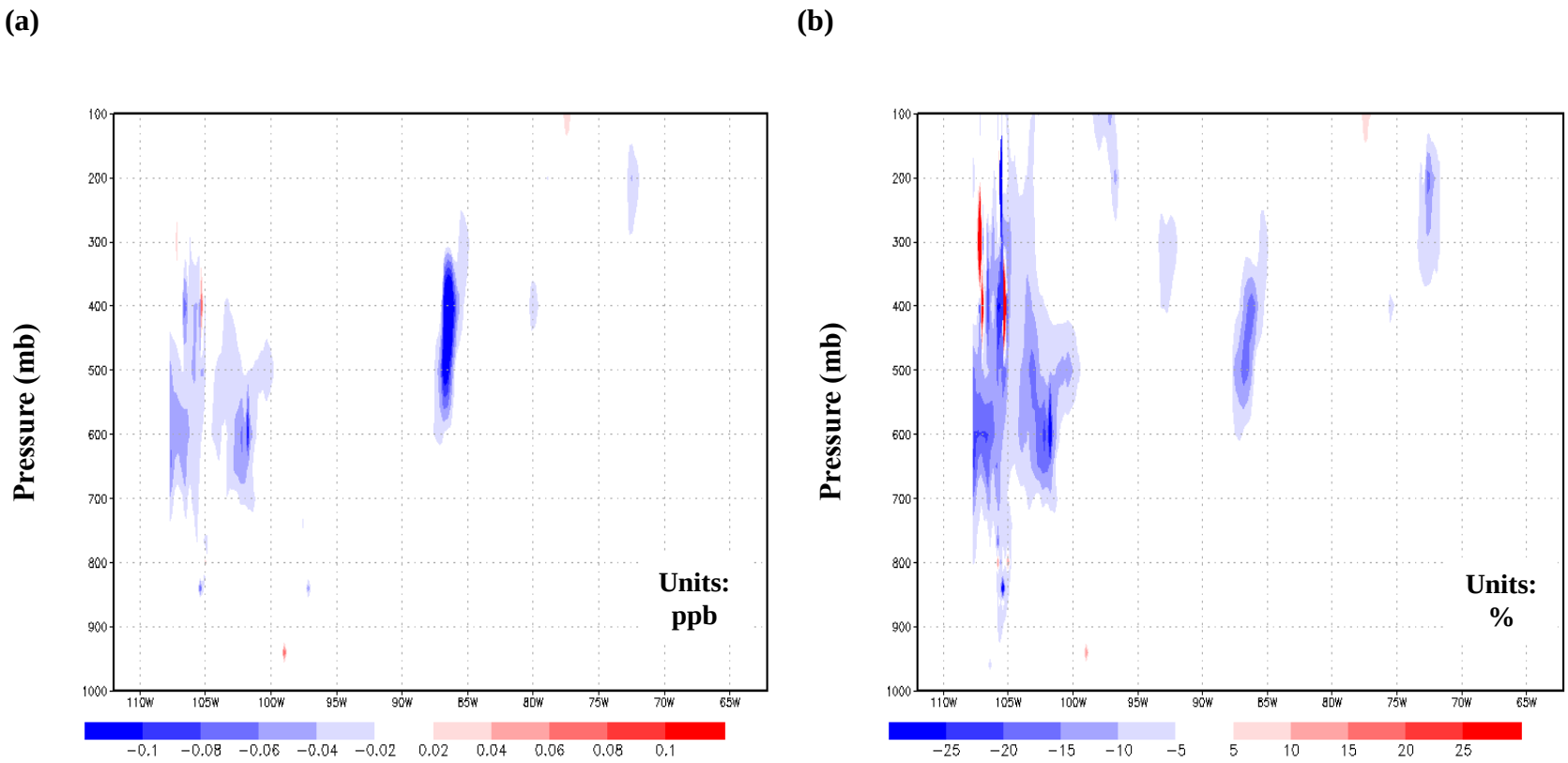

Figure 8 – Vertical cross section of absolute differences (ppb) (a) and percent differences (b) in gas phase HNO_3 concentration between 25% partitioning case and LNO_x case from 1000 mb to 100 mb at 33°N for 10Z on August 23rd. The spatial extent and magnitude of the absolute and percent differences were slightly smaller than in the 100% partitioning case (Figures 6a and 6b).

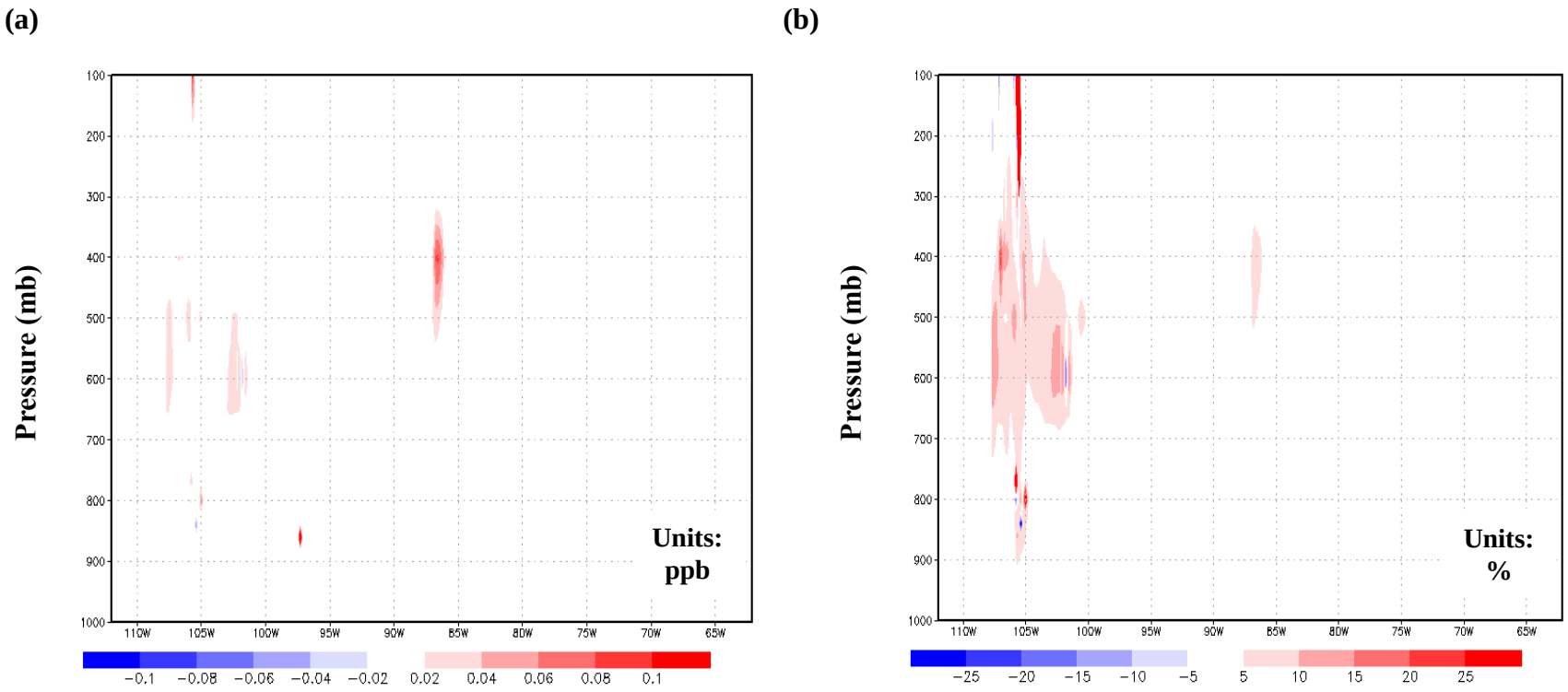

Figure 9 – Vertical cross section of absolute differences (ppb) (a) and percent differences (b) in gas phase HNO_3 concentration between 25% partitioning case and 100% partitioning case from 1000 mb to 100 mb at 33°N for 10Z on August 23rd. While there were differences between the two partitioning case, overall, the two cases were fairly similar.

Changes in NO_x and O_3

Similar to how the addition of lightning-produced NO_x increased gas phase HNO_3 concentrations (Figure 2), changes in gas phase HNO_3 influenced NO_x (NO_2 + NO) concentrations. As expected, NO_x concentrations decreased in areas where gas phase HNO_3 decreased due to ice partitioning. Figure 10 illustrates the percent change in gas phase NO_x between the 100% partitioning case and LNO_x case for 0Z on August 12th at 400 mb. Decreases in NO_x were generally less than 10%, with some scattered regions where decreases were near 20%. An area of decreases near 10% was located in northern Mexico in the 100% partitioning case (Figure 10). This area was spatially similar to the relatively large differences in gas phase HNO_3 for the same time and pressure level (Figures 4a and 4b).

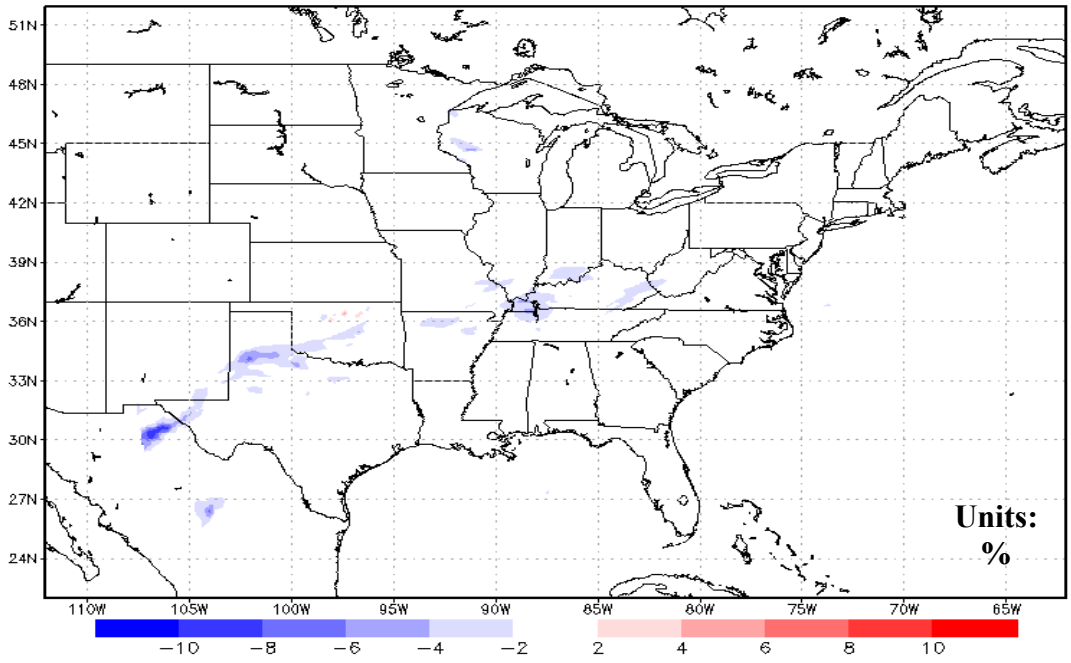

Figure 10 – Percent differences in NO_x concentration between 100% partitioning case and LNO_x case at 400 mb for 0Z on August 12th. The largest decreases in NO_x were spatially similar to the regions where the large differences in gas phase HNO_3 occurred for a given time and pressure level.

No substantial changes in O_3 were seen at any level throughout the time period. The maximum decreases in O_3 observed throughout the two weeks were less than 1%. For 0Z on August 12th at 400 mb, decreases in ozone were less than 0.2% for most of the domain (see Appendix A, Figure S-4).

Changes in HONO

Changes in HONO were spatially similar to the changes in NO_x. Reductions in gas phase HONO concentration were typically less than 10% for both ice partitioning cases, with some areas having decreases near 20%. Figure 11 represents a vertical cross section for the percent difference in HONO concentration between the 100% partitioning case and the LNO_x case at 30°N for 23Z on August 25th. Decreases larger than 10% occurred near 400 mb at 75°W, with decreases near 10% between 100 and 200 mb.

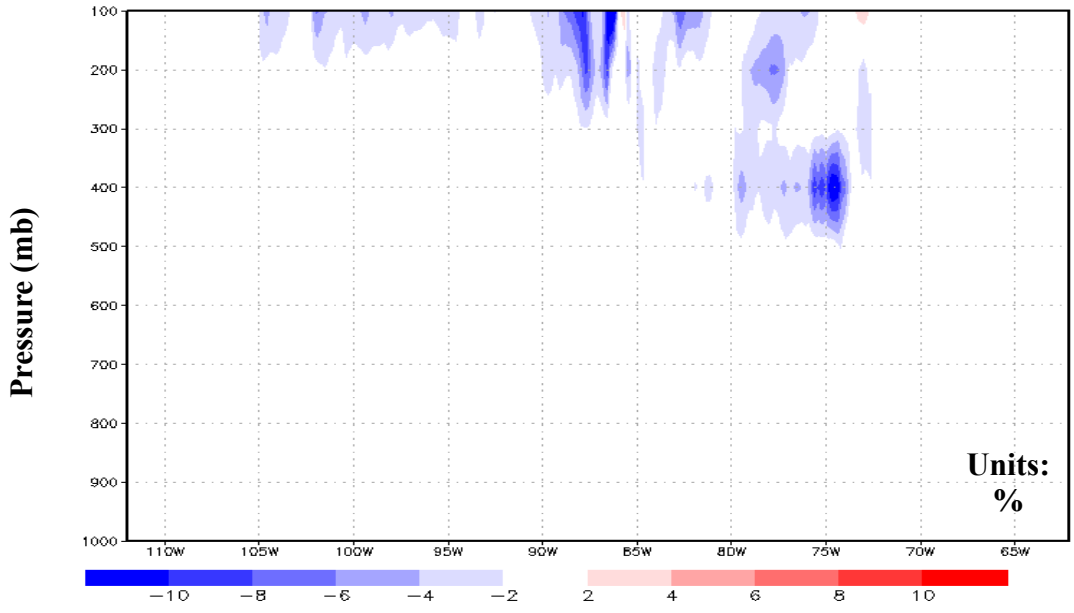

Figure 11 – Vertical cross section of percent differences in HONO concentration between 100% partitioning case and LNO_x case from 1000 mb to 100 mb at 30°N. Figure is for 23Z on August 25th. Peak decreases in HONO during the two week period were generally less than 20%.

Changes in Particulate Nitrate

Changes in gas phase HNO_3 and nitrate mass concentration were generally not spatially similar vertically or horizontally. Adsorbed gas phase HNO_3 was removed by cloud ice and partitioned to the aerosol phase. Some of the most noticeable increases in particulate nitrate mass concentrations were present at 100 mb during the two week period. Unlike the other pressure levels included in this work, 100 mb is assumed to be located within the stratosphere. Increases in nitrate at 100 mb were often just as large as or greater than changes at 300 mb and 400 mb, where decreases in gas phase HNO_3 were higher. At 0Z on August 12th, increases in accumulation mode nitrate between the 100% partitioning case and the LNO_x case for 100 mb were visible over parts of southern New Mexico and central Indiana, which is exhibited in Figure 12. Peak changes in the mass concentration in these regions were as high as 0.15 µg/m^3.

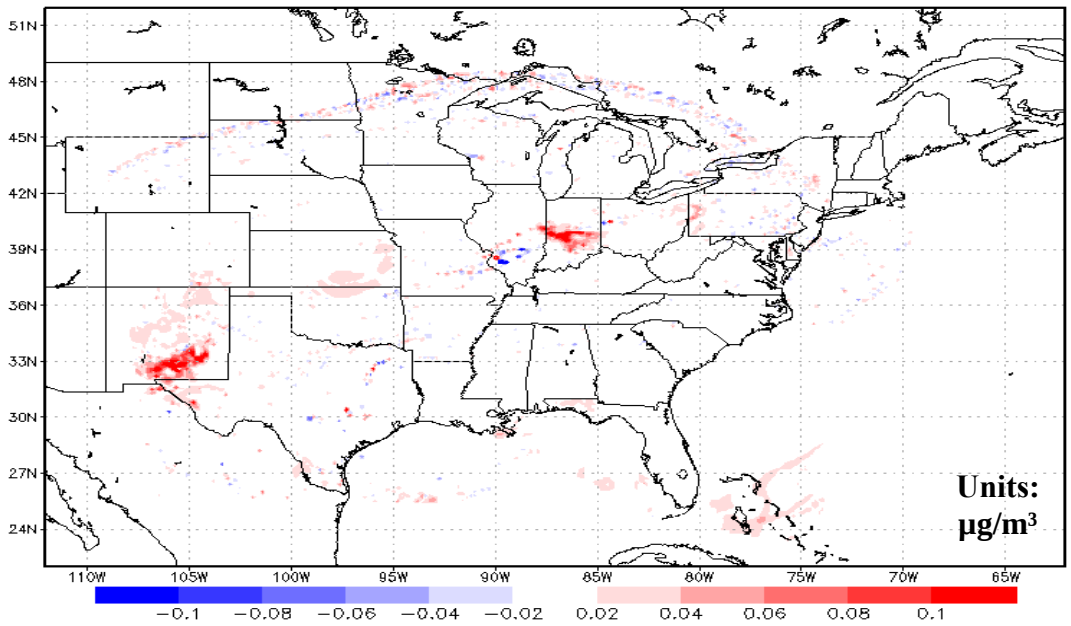

Figure 12 – Absolute differences in accumulation mode nitrate mass concentration (µg/m³) between 100% partitioning case and LNO_x case at 100 mb for 0Z on August 12th. Changes in the nitrate mass concentration were vertically higher than the changes in gas phase HNO_3 for the same time (Figure 4a).

Figures 13a and 13b illustrate these changes in accumulation mode mass concentration for the same level and time as Figure 12, where Figure 13a shows the nitrate mass concentration for the LNO_x case and Figure 13b shows the nitrate mass concentration for the 100% partitioning case. As in Figure 12, southern New Mexico and central Indiana stand out as the region where substantial increases were seen. Other areas such as northern Oklahoma and western Pennsylvania also had detectible differences between the two cases. For the 25% partitioning case, considerable changes were still evident for this time and pressure level (Figure 14). The changes in nitrate mass were slightly smaller in magnitude and less widespread. Nevertheless, increases in nitrate mass concentration were greater than 0.10 $\mu g/m^3$ for parts of southern New Mexico and central Indiana (Figure 14). Similar changes in particulate nitrate mass were observed for 23Z on August 25th at 100 mb (not shown).

(a) **(b)**

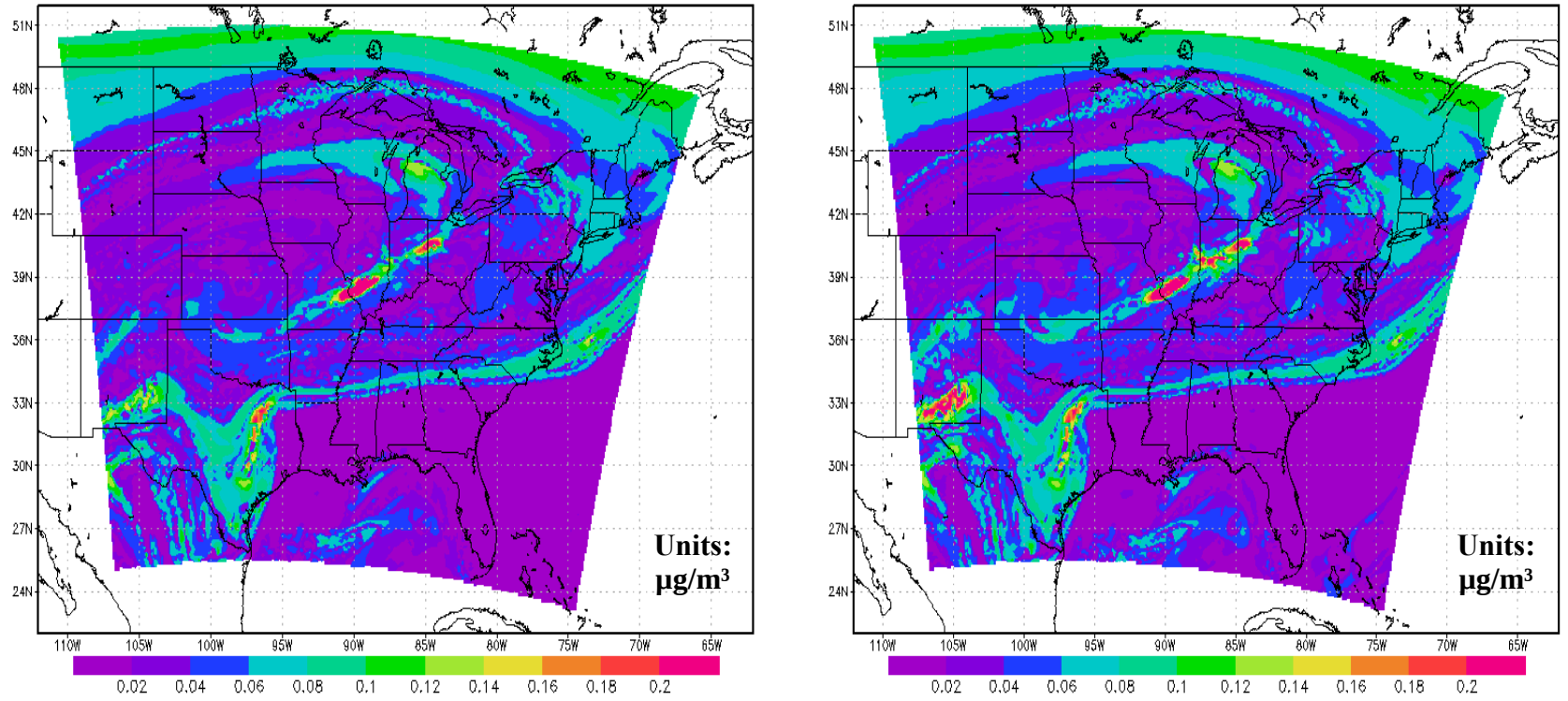

Figure 13 – Accumulation mode nitrate concentration (µg/m³) for LNO_x case (a) and 100% partitioning case (b) at 100 mb for 0Z on August 12th. Considerably larger mass concentrations were seen in 100% partitioning case in southern New Mexico and central Indiana.

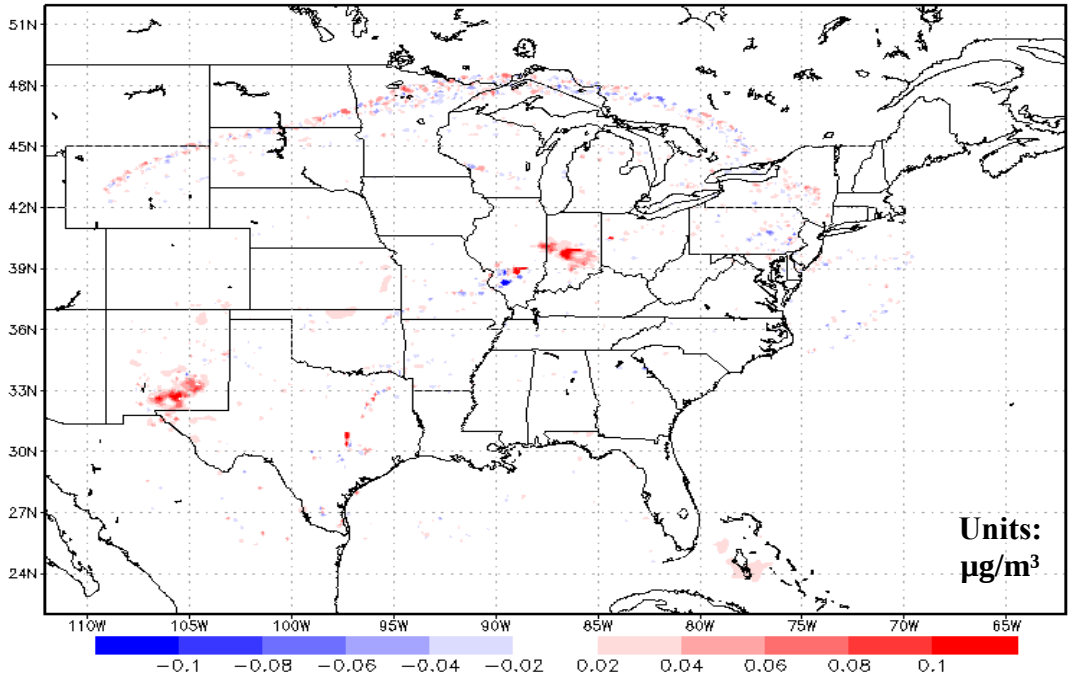

Figure 14 – Absolute differences in accumulation mode nitrate mass concentration (µg/m³) between 25% partitioning case and LNO_x case at 100 mb for 0Z on August 12th. The spatial extent and magnitude of the absolute differences were slightly smaller than in the 100% partitioning case (Figure 12).

Regions of maximum increase in nitrate mass concentration often did not correspond to areas where gas phase HNO_3 was removed. For 200 mb, 300 mb and 400 mb, increases in particulate nitrate were more likely to be found in the northern and central regions of the domain. This is illustrated in Figures 15a and 15b. Both figures are for 200 mb at 21Z on August 18th. In Figure 15a, decreases in gas phase HNO_3 were found in parts of northern Mexico and southern Texas. However, in Figure 15b, the increases in nitrate were found mainly in Wisconsin.

(a) **(b)**

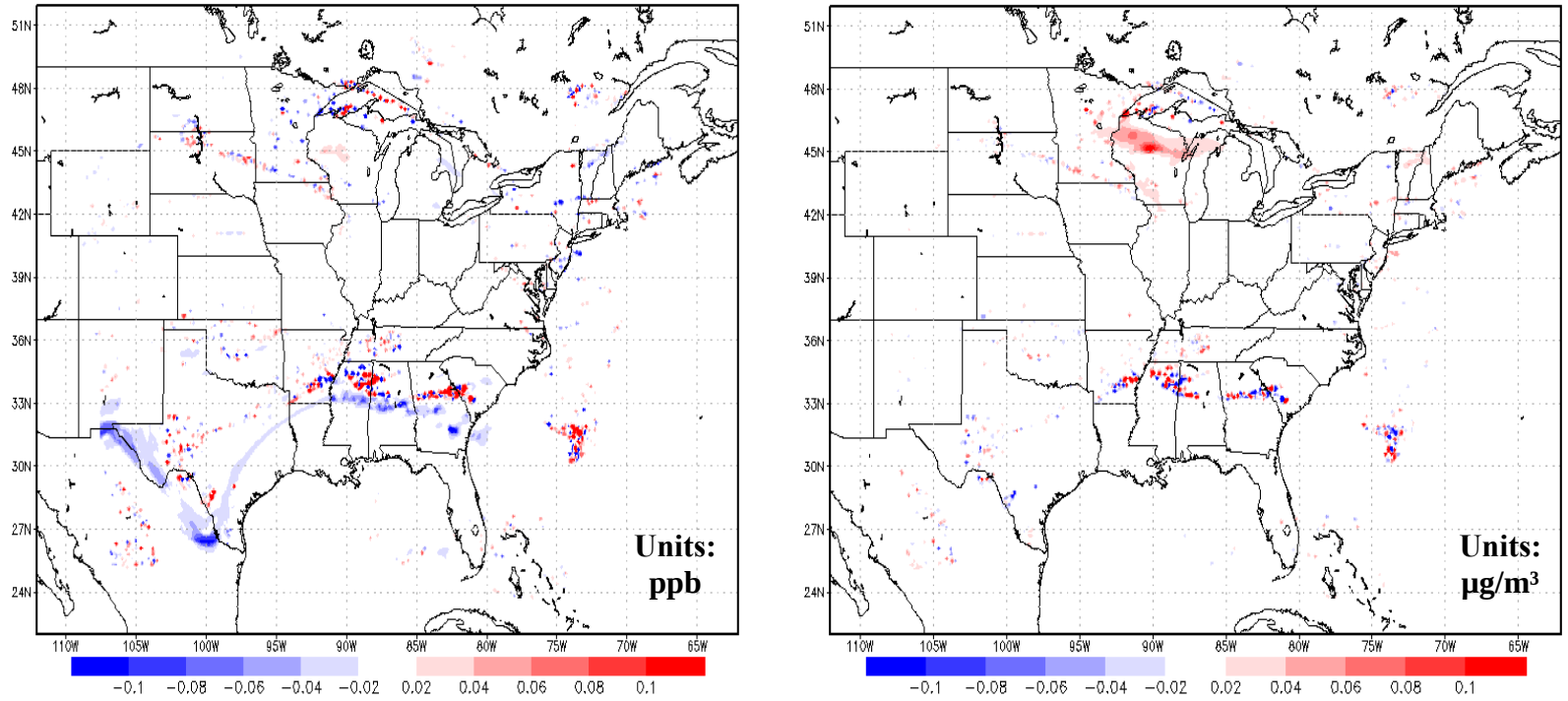

Figure 15 – Absolute differences in gas phase HNO_3 concentration (ppb) (a) and accumulation mode nitrate mass concentration (µg/m³) (b) between 100% partitioning case and LNO_x case at 200 mb for 21Z on August 18th. Decreases in gas phase HNO_3 were found in parts of northern Mexico and southern Texas, while the increases in particulate nitrate were found mainly in Wisconsin.

Changes in SO_2, H_2O_2 and Sulfate

No substantial changes were observed from the inclusion of SO_2 and H_2O_2 partitioning and the subsequent reaction to form sulfate. Maximum changes in sulfate aerosol mass concentrations were ten orders of magnitude less than sulfate mass concentrations. No substantial changes in SO_2 and H_2O_2 in the gas phase were observed, suggesting reactive uptake, as implemented here, did not occur on a time scale sufficient for appreciable accumulation of sulfate mass in the particle phase.

Discussion

Gas Phase HNO_3

With changes of over 25% in scattered regions, the partitioning of gas phase HNO_3 to ice can be an important process occurring in the upper troposphere during the summer, and thus should be added to CMAQ. While it is expected that this would be most important at the levels where cloud ice is more prevalent (300 mb and 400 mb), considerable amounts of HNO_3 partitioned to ice at altitudes as low as 650 mb when both ice and HNO_3 were present.

Past studies found larger amounts of HNO_3 partitioning to ice than predicted here (Popp et al., 2004, Krämer et al., 2008, Marécal et al., 2010). Peaks in ice mixing ratio and gas phase HNO_3 concentration rarely coincided (Figures 3a and 3b) during this two week simulation. It is possible that at different time periods, greater percentages of gas phase HNO_3 could be removed. This is due to the fact that this process is dependent on both gas phase HNO_3 and cloud ice being co-located in time and space. There are also uncertainties regarding CMAQ's ability to accurately predict gas phase HNO_3 concentrations in the upper levels of the atmosphere. It was recently noted by Henderson et al. (2011) that CMAQ under predicted measured NO_x concentrations aloft by more than 30%, suggesting upper level predictions of HNO_3 are unreliable.

Though the extent to which HNO_3 ice partitioning is reversible remains debated, most estimates in the literature propose somewhere between 25% and 100% remains in the condense phase. Considerable decreases in gas phase HNO_3 were present in both sensitivity simulations, suggesting this pathway should be added to CMAQ, but more aloft measurements are needed to validate the model approach.

Particulate Nitrate

Changes in particulate nitrate mass concentrations were present throughout the time period in the upper levels of the atmosphere, suggesting important implications for climate and long-range pollution transport. These increases were seen at the levels where gas phase HNO_3 partitioned to ice, but also above at 100 mb. Two interesting observations regarding particulate nitrate were noted throughout the two week period. First, changes in particulate nitrate often were not spatially similar vertically or horizontally to areas where gas phase HNO_3 was removed. Second, especially for 200 mb, 300 mb and 400 mb, increases in nitrate were consistently found in the northern and central regions of the domain. This occurred even when the largest changes in gas phase HNO_3 were found in the southern regions of the domain.

A potential explanation for these spatial differences might be the ratio of total ammonia to total sulfate, and the subsequent influence on aerosol acidity and HNO_3 partitioning preference. In ammonia poor areas ([total ammonia] < 2[total sulfur]), the atmospheric aerosol is more acidic (Seinfeld and Pandis, 2006). This causes nitrate to partition from the aerosol phase to the gas phase. In the ammonia-rich regime ([total ammonia] > 2[total sulfur]), the partitioning of HNO_3 from the gas phase to form ammonium nitrate is favored. This ratio of total ammonia to total sulfate may affect whether or not the gas phase HNO_3 that adsorbed to ice remains partitioned to the aerosol phase. If the uptake by ice occurs in an ammonia rich area, the partitioning from the gas phase to the aerosol phase will be favored. Greater ammonium aerosol concentrations in the northern U.S could be the reason why partitioning to the aerosol phase was more likely to occur in this region (see Appendix A, Figure S-5). However, if gas phase HNO_3

adsorbs to ice in an ammonia poor area, HNO_3 will partition back to the gas phase at a later time step. This might explain why we often did not observe the partitioning of gas phase HNO_3 to nitrate in the southern regions of the U.S., where ammonium aerosol mass concentrations were frequently smaller (Figure S-5).

Another explanation for changes in nitrate concentrate might relate to CMAQ re-establishing equilibrium between the gas phase and aerosol modes (Aitken, accumulation and coarse). Up until this point, all figures regarding nitrate have been for the accumulation mode. Figure 16 is the same as Figure 12, except that it is for Aitken mode nitrate. Both figures are for 0Z on August 12th at 100 mb. Where there were increases in mass concentration in the accumulation mode (Figure 12), there were decreases in the Aitken mode mass (Figure 16), and the areas of respective increases and decreases correspond spatially and temporally. Similar results were also present in the 25% partitioning case.

Figure 17 represents the three aerosol modes in CMAQ, and how nitrate and gas phase HNO_3 partition back and forth between the aerosol phase and gas phase. If gas phase HNO_3 decreases, nitrate will be drawn out of the aerosol phase to re-establish equilibrium. This attempt to re-establish equilibrium between the different aerosol modes and gas phase HNO_3 in CMAQ could be producing this pattern in nitrate concentration seen in Figures 12 and 16. When the total NO_3 (gas phase HNO_3 plus total particulate nitrate) concentration for the LNOx case was compared to the 100% partitioning case at 200 mb for 21Z on August 18th, the two were very similar. Any differences between the two cases were less than 0.10 $\mu g/m^3$ (see Appendix A, Figures S-6a and S-6b).

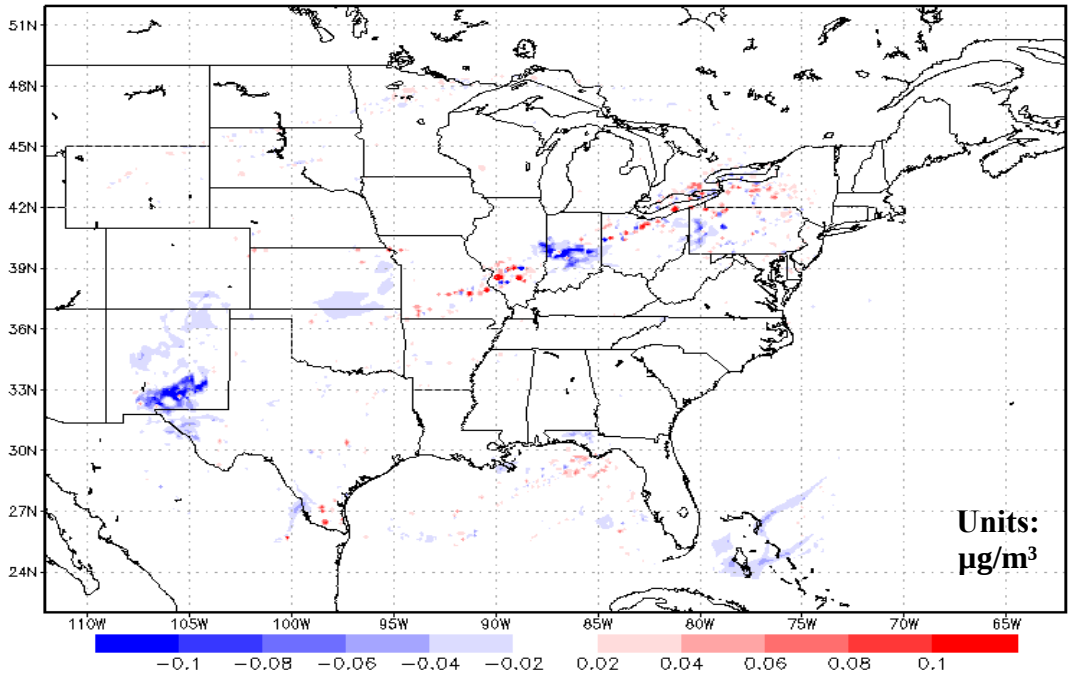

Figure 16 – Absolute differences in particulate nitrate mass concentration (Aitken mode) between 100% partitioning case and LNO_x case at 100 mb for 0Z on August 12th. Where there were decreases in the Aitken mode mass, there were increases in the accumulation mode mass (Figure 12). These areas of respective increases and decreases between the two aerosol modes correspond spatially and temporally.

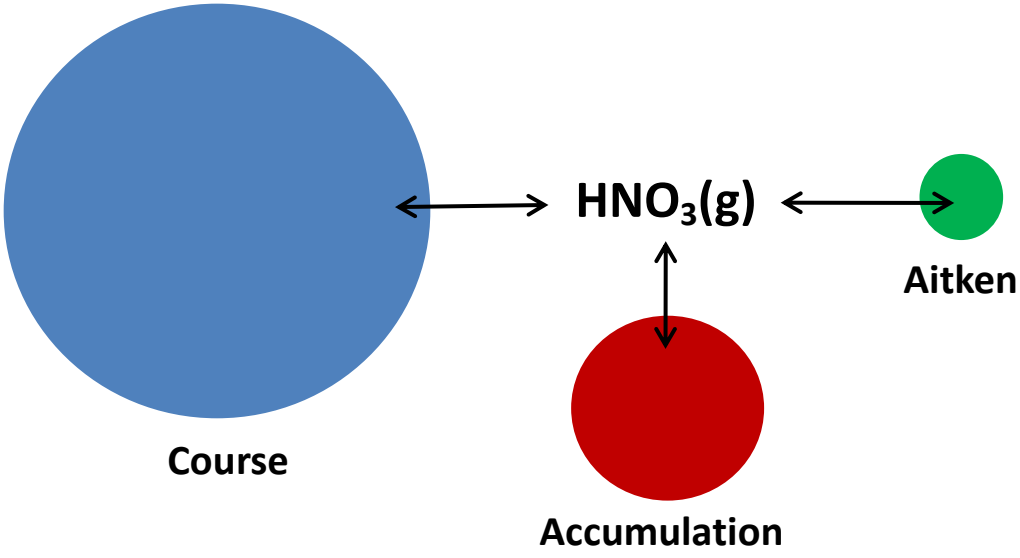

Figure 17 – This figure shows the three different aerosol modes in CMAQ, and how nitrate and gas phase HNO_3 partition back and forth between the aerosol phase and gas phase. When there are decreases in gas phase HNO_3, nitrate will be drawn out of the aerosol phase to re-establish equilibrium.

Changes in predicted nitrate aerosol concentration are important because of potential effects on radiative forcing, climate and long range pollution transport. Not only is the overall mass concentration of nitrate an important factor, but the size distribution and vertical placement of the nitrate aerosol affect radiative forcing and transport calculations.

SO_2, H_2O_2 and Sulfate

After Clegg and Abbatt (2001b) suggested the possible reaction between SO_2 and H_2O_2, it is interesting to consider why no sulfate was found to form via ice chemistry in the CMAQ simulations. It is important to note that SO_2 concentrations in the upper parts of the troposphere are much lower than Clegg and Abbatt used in their experiment. It may also be that ice mixing ratios and gas phase concentrations of SO_2 and H_2O_2 were not all co-located in space and time. Thus, without considerable amounts of all three, reaction rates would be slower and low amounts of sulfate would form. In addition, this reaction is hindered by the smaller partitioning coefficients of SO_2 and H_2O_2 when compared to other gases such as HNO_3. As a result, reaction rates were too slow for the adsorbed SO_2 and H_2O_2 to react on the surface of the ice. The very small amounts of sulfate resulting from the reaction as implemented in this experiment suggest that the reaction between SO_2 and H_2O_2 on ice is not a substantial contributor to sulfate mass in the atmosphere. Thus for the summer of 2005, there are likely other processes explaining why sulfate was under predicted in Appel (2010).

Limitations

The conclusions drawn in this work are limited by uncertainty and simplifications. Parameters (A_p and B_p) for the partition coefficients (Table 1) were empirically derived for particular temperature and pressure ranges, but used at all conditions for which there was cloud ice. This implementation in CMAQ resulted in extrapolation where cloud ice was present at temperatures outside these ranges.

For simplicity, ice particles shapes were assumed to be spheres. While this is useful as a lower limit, assuming all ice crystals are spheres is not an accurate representation of cloud ice in the atmosphere. An additional simplification made in this work was that it was assumed that the ice surface was never limiting. Thus, competition between the gases was not taken into account. In the actual atmosphere, many gases compete for space to adsorb to. Unlike the spherical ice shape simplification, this is not a lower bound estimate.

Future Directions

As mentioned in Marécal et al. (2010), trapping theory may be an important process for the redistribution of HNO_3. Trapping theory assumes that when an ice particle grows from the deposition of water, a gas that has adsorbed to the surface of that ice will be trapped in the bulk of the ice. Thus, the gas is trapped until the ice particle evaporates. If this process is important, it could potentially affect NO_x and O_3 concentrations in the upper troposphere.

Since ice crystals were assumed to be sphere, a future direction for this work would be to use different shapes. Possible shapes for ice crystals include needles, hexagonal plates, columns and dendrites. While this study only included ice crystals, it is possible that the uptake by other frozen hydrometeors, including snow and hail, is also important (Marécal et al. 2010). Other gases that also partition efficiently to ice, such as HCl, may also be interesting to study. By including a gas such as HCl, competition between the HNO_3 and HCl could be considered.

Another important direction would be improving measurements of upper tropospheric gases such as HNO_3, NO_x and O_3. This would help us confirm model predictions. While it might prove to be difficult, a field study determining the amount of adsorbed HNO_3 that partitions to the condense phase and stays in the condense phase would significantly improve our understanding of this process.

Conclusion

Based on the findings of this work, the partitioning of gas phase HNO_3 to ice may be an important atmospheric process for the summer months. Decreases in gas phase HNO_3 concentration were as high as 25% in CMAQ when comparing the LNO_x case to the two partitioning (100% and 25%) simulations. This in turn had an influence on NO_x and HONO concentrations (up to 20% decreases) in the upper parts of the troposphere. However, O_3 concentrations were insensitive to decreases in gas phase HNO_3 due to ice partitioning. Also increases in particulate nitrate mass due to the condensing of gas phase HNO_3 were as high as 0.15 $\mu g/m^3$. These changes in nitrate mass concentration could potentially pose a negative forcing on climate and affect long range pollution transport. Consistent with Clegg and Abbatt (2001a), we found that the scavenging of SO_2 and H_2O_2 by ice particles was very small. When considering the reaction of the two to form sulfate, increases in sulfate concentrations were negligible.

Appendix A – Supplemental Figures

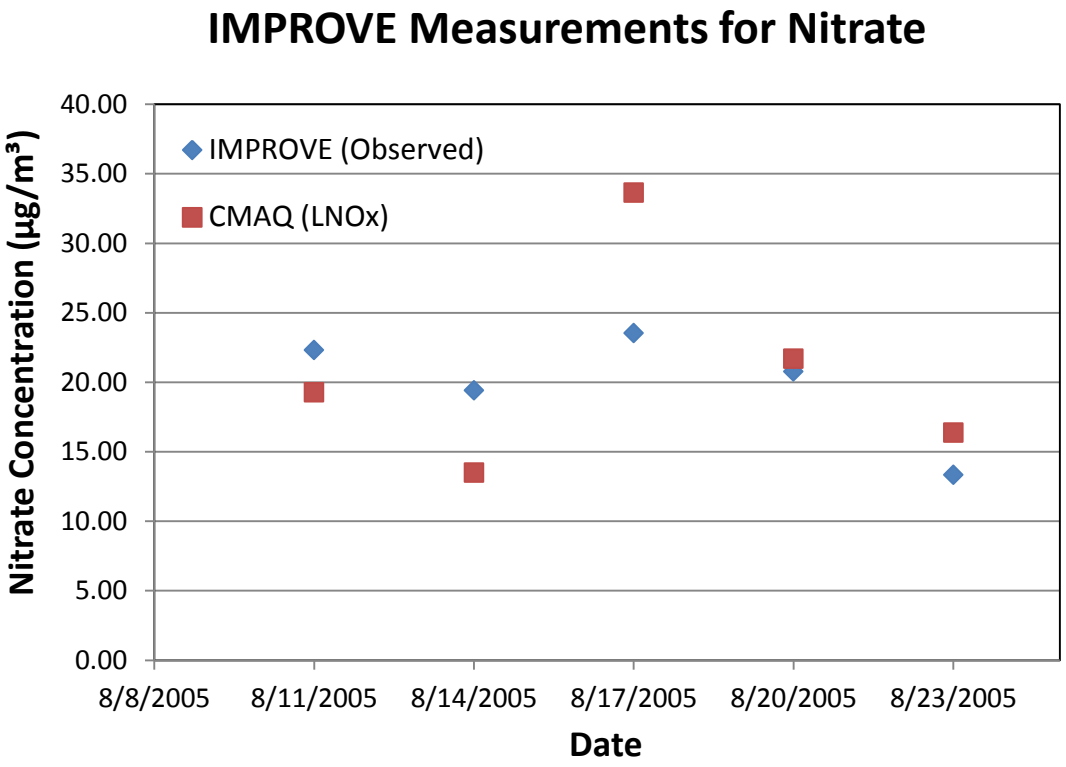

Figure S-1 – Daily average nitrate measurements (µg/m³) for all IMPROVE sites and corresponding predictions grid cells in CMAQ for 5 days (11th, 14th, 17th, 20th, and 23rd) in August of 2005. A small normalized mean bias of 1.03% was found between CMAQ and the IMPROVE observations. A fairly large over prediction by the CMAQ was seen for August 17th.

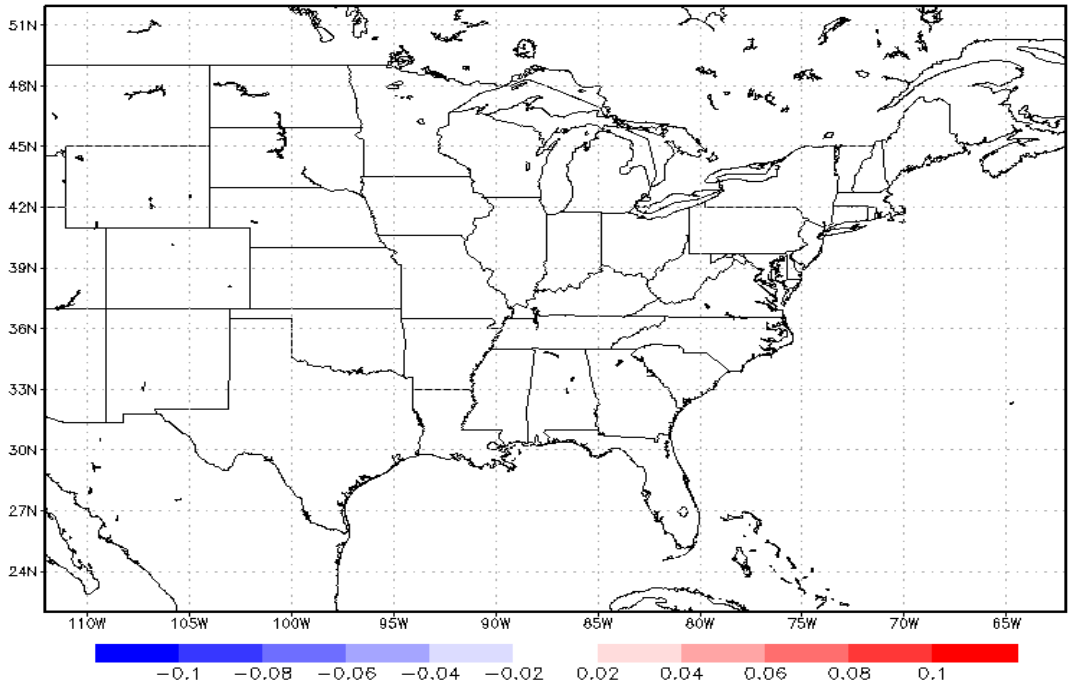

Figure S-2 – Absolute difference plot between two different simulations of the 100% ice partitioning case. The constant white shows there are no differences between the two simulations for 23Z on August 10th for 400 mb. This supports the claim that there was very little numerical noise.

(a) **(b)**

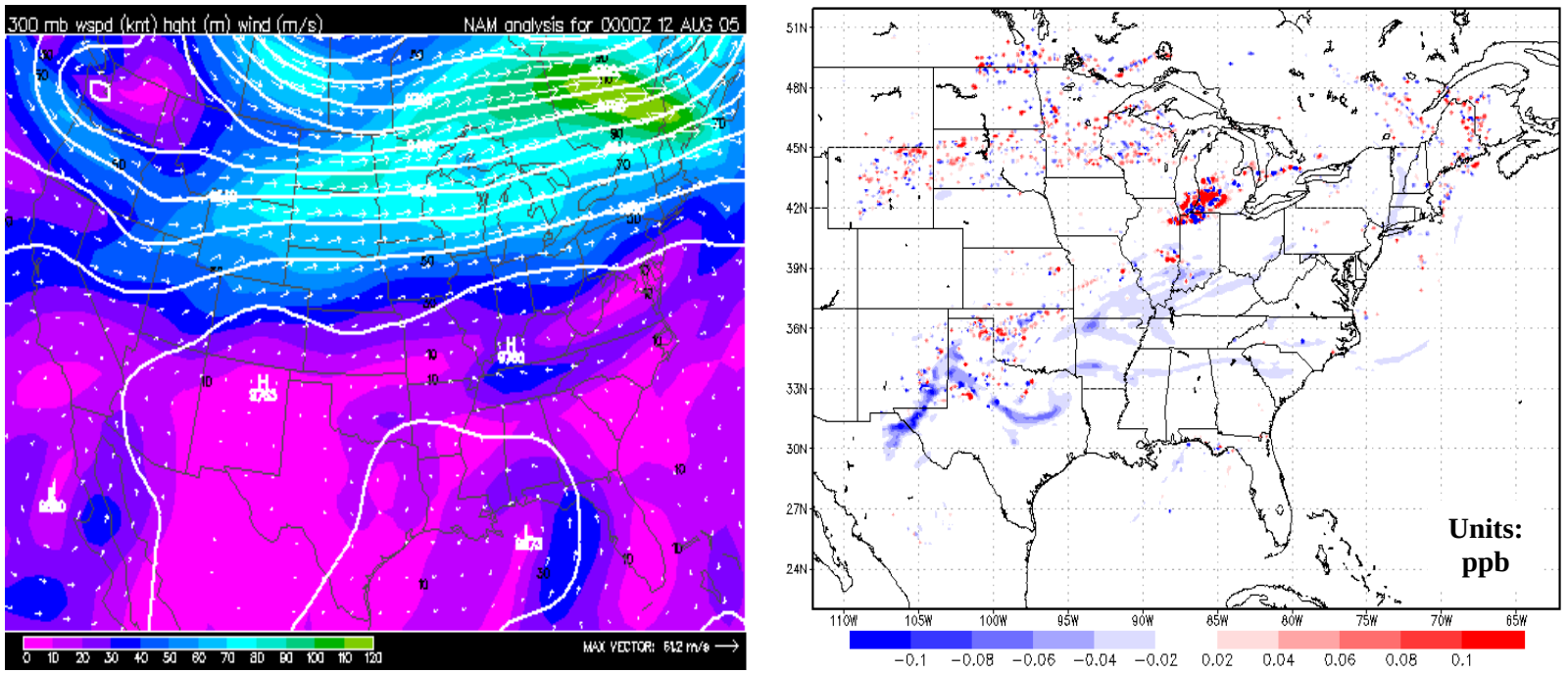

Figure S-3a – Wind speeds in m/s shading for 0Z on August 12th at 300 mb. White arrows show wind direction and white contours display heights in meters. Largest wind speeds are located in the northern central U.S. and Canadian province of Quebec. These regions correspond to where the largest alternating patterns of HNO_3 differences are located in Figure S-3b (This figure appears courtesy of Unisys Weather: http://weather.unisys.com/).

Figure S-3b – Absolute differences in gas phase HNO_3 concentration (ppb) between 100% partitioning case and LNO_x case at 300 mb for 0Z on August 12th

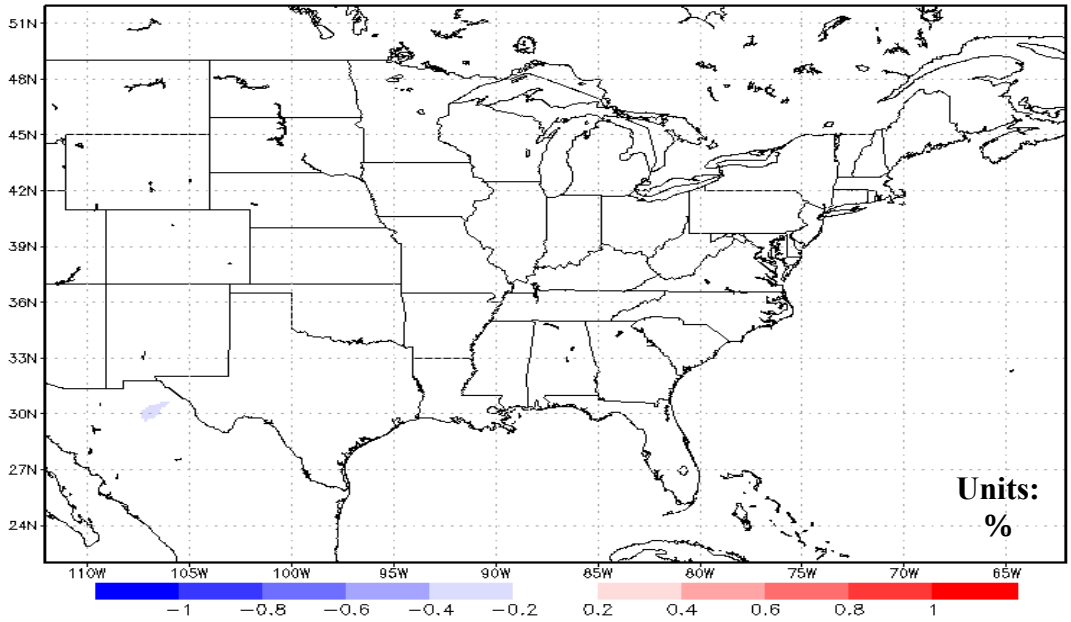

Figure S-4 – Percent differences in O_3 concentration between 100% partitioning case and LNO_x case at 400 mb for 0Z on August 12th. Very small decreases in O_3 were seen at this time and throughout the period. O_3 concentrations were insensitive to decreases in gas phase HNO_3 due to ice partitioning.

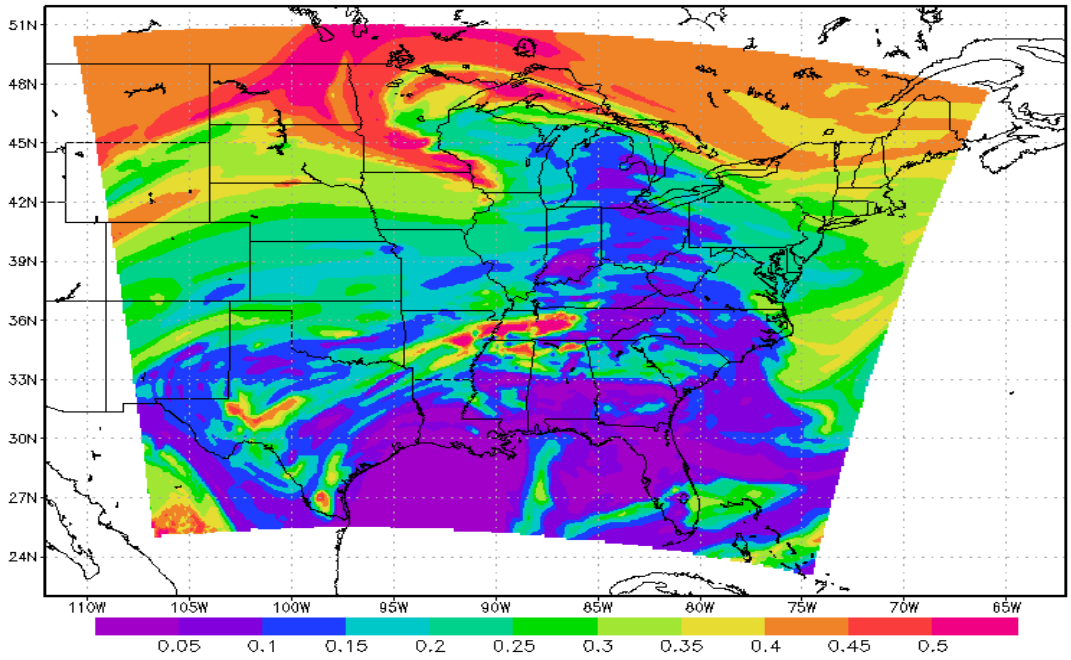

Figure S-5 – Ratio between ammonium aerosol and sulfate aerosol at 200 mb for 21Z on August 18th. Ratios are unit less. Ammonium aerosol concentrations were generally larger in the northern regions of the domain and smaller in the southern regions.

(a) **(b)**

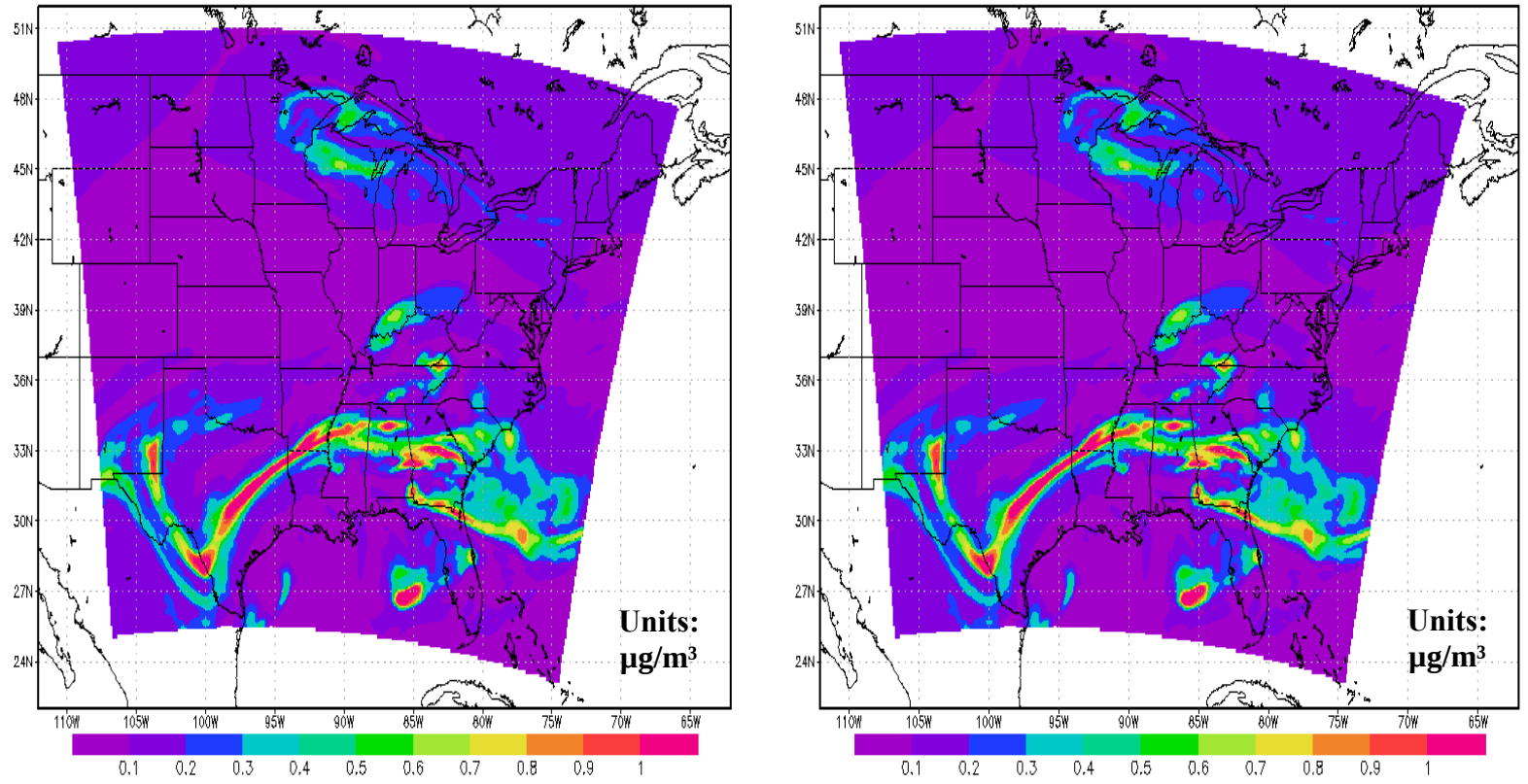

Figure S-6 – Total NO_3 (gas phase HNO_3 plus total particulate nitrate) concentration (µg/m³) for LNOx case (a) and 100% partitioning case (b) at 200 mb for 21Z on August 18th. The two cases were very similar. Any differences between the two cases were less than 0.10 µg/m³.

Appendix B - Amendments Made to CMAQ Code

All changes made to the ***cldproc_acm.F*** subroutine. CMAQ code is written in FORTRAN.

```
REAL    ADS_HNO3_RATIO                ! ratio of HNO3 that adsorbed to ice
REAL    Klin_HNO3                     ! partition (to ice) coefficient for HNO3 (m)
REAL    REMOV_ICE_HNO3                ! amount of HNO3 removed by only ice
REAL    ADS_SO2_RATIO                 ! ratio of SO2 that adsorbed to ice
REAL    ADS_ICE_SO2                   ! amount of SO2 adsorbed to surface of ice (moles/L or M)
REAL    REACT_SO2                     ! change in SO2 due to reaction on ice in (moles/L or M)
REAL    DELSO2                        ! change in SO2 due to reaction on ice in mixing ratio
REAL    Klin_SO2                      ! partition (to ice) coefficient for SO2 (m)
REAL    REMOV_ICE_SO2                 ! amount of SO2 removed by only ice
REAL    ADS_H2O2_RATIO                ! ratio of H2O2 that adsorbed to ice
REAL    ADS_ICE_H2O2                  ! amount of H2O2 adsorbed to surface of ice (moles/L or M)
REAL    REACT_H2O2                    ! change in H2O2 due to reaction on ice in (moles/L or M)
REAL    DELH2O2                       ! change in H2O2 due to reaction on ice in mixing ratio
REAL    Klin_H2O2                     ! partition (to ice) coefficient for H2O2 (m)
REAL    REMOV_ICE_H2O2                ! amount of H2O2 removed by only ice
REAL    REACT_H2SO4                   ! change in H2SO4 conc due to reaction on ice
REAL    DELH2SO4                      ! change in H2SO4 conc due to reaction on ice
REAL    KH2SO4                        ! reaction rate constant for H2SO4 reaction (M-2 s-1) (Ervens et al. 2004)
REAL    SAICE                         ! total surface area of ice particles (m2/m3)
REAL    TA( NCOLS, NROWS, NLAYS )     ! air temperature (K)
REAL    QI( NCOLS, NROWS, NLAYS )     ! ice content (kg/kg)
REAL    NCONC_ICE                     ! number conc. of ice (m-3)
REAL    NEW_TA                        ! air temperature in celsius
REAL    PRES( NCOLS, NROWS, NLAYS )   ! air pressure (Pa)
REAL    REFF                          ! ice effective radius (m) (Mather et al., 2007)
REAL    TAUCLD                        ! cloud lifetime (sec)
REAL    VOLICE                        !Volume of an ice with of radius = effective radius
```

```
C... Partitioning to ice

      DO LAY = 1, NLAYS
        DO ROW = 1, MY_NROWS
          DO COL = 1, MY_NCOLS

C… Solve for ice surface area
            NEW_TA = TA( COL, ROW, LAY ) - 273.15                    ! convert from Kelvin to Celsius
            REFF = ( (75.3 + ( 0.5895 * NEW_TA ) ) / 2 ) * 1E-6      ! effective radius of ice (m)
            VOLICE = ( ( 4 * 3.141592 ) / 3) * ( REFF ** (3.) )
             NCONC_ICE = ( ( QI( COL, ROW, LAY ) ) / ( VOLICE  * ( ICEDENS / DENS( COL, ROW, LAY ) ) ) )
             SAICE = ( ( 4 * 3.141592 * ( REFF ** (2.) ) ) * NCONC_ICE )         ! ice surface area (m2/m3)

C… Solve for partitioning coefficients
            IF ( SAICE .GT. 0.0 ) THEN
              IF( TA( COL, ROW, LAY ) .LT. 273.15 ) THEN
                Klin_HNO3 = ( 7.5E-07 ) * EXP ( 4585 / ( TA( COL, ROW, LAY ) ) )       ! partition (to ice) coefficient for HNO3 (m)
                Klin_SO2 = ( 7.3E-06 ) * EXP ( 2065 / ( TA( COL, ROW, LAY ) ) )        ! partition (to ice) coefficient for SO2 (m)
                Klin_H2O2 = ( 2.1E-07 ) * EXP ( 3800 / ( TA( COL, ROW, LAY ) ) )           ! partition (to ice) coefficient for H2O2 (m)

              ELSE
                Klin_HNO3 = 0
                Klin_SO2 = 0
                Klin_H2O2 = 0
              END IF

C… Code for HNO3 adsorbing to ice and partitioning to aerosol phase (accumulation mode nitrate)

              SPC = 0
              DO SPC = 1, NSPCSD
```

```
          IF (SPC .EQ. 10) THEN                                                    ! SPC 10 = HNO3
          REMOV_ICE_HNO3 = ( SAICE * Klin_HNO3 * CGRID( COL, ROW, LAY, 10 ) )   ! amount of HNO3 partitioning to ice

           IF ( REMOV_ICE_HNO3 .LE. CGRID( COL, ROW, LAY, 10 ) ) THEN
                        REMOV_ICE_HNO3 = REMOV_ICE_HNO3
           ELSE
            REMOV_ICE_HNO3 = CGRID( COL, ROW, LAY, 10 )
           END IF

           REMOV_ICE_HNO3 = ( 1 * ( REMOV_ICE_HNO3 ) )                    ! either 1 or .25 (for 25% partitioning case)
           ADS_HNO3_RATIO = ( REMOV_ICE_HNO3 ) / ( CGRID( COL, ROW, LAY, 10 ) )
           CGRID( COL, ROW, LAY, 10 ) = CGRID( COL, ROW, LAY, 10 ) - REMOV_ICE_HNO3       ! new end conc for HNO3

          END IF

          IF (SPC .EQ. 78) THEN                                                  ! SPC 78 = accumulation mode nitrate
           CGRID( COL, ROW, LAY, 78 ) = CGRID( COL, ROW, LAY, 78 ) + ( REMOV_ICE_HNO3 )         ! new cend conc for
ANO3J
          END IF

         END DO

C… Code for SO2 and H2O2 reaction

         SPC = 0
         DO SPC = 1, NSPCSD

          IF (SPC .EQ. 13) THEN                                                  ! SPC 13 = H2O2
           REMOV_ICE_H2O2 = ( SAICE * Klin_H2O2 * CGRID( COL, ROW, LAY, 13 ) )   ! amount of H202 partitioning to ice
           IF ( REMOV_ICE_H2O2 .LE. CGRID( COL, ROW, LAY, 13 ) ) THEN
            REMOV_ICE_H2O2 = REMOV_ICE_H2O2
```

```
            ELSE
              REMOV_ICE_H2O2 = CGRID( COL, ROW, LAY, 13 )
            END IF

            ADS_H2O2_RATIO = ( REMOV_ICE_H2O2 ) / ( CGRID( COL, ROW, LAY, 13 ) )

            ADS_ICE_H2O2 = ( ( REMOV_ICE_H2O2 * ( ( PRES ( COL, ROW, LAY ) ) / ( UNIVERR * TA( COL, ROW, LAY ) )
) ) / 1000 )                                                    ! convert to moles/L or M

          END IF

          IF (SPC .EQ. 52) THEN                                                    ! SPC 52 = SO2
            REMOV_ICE_SO2 = ( SAICE * Klin_SO2 * CGRID( COL, ROW, LAY, 52 ) )      ! amount of SO2 partitioning to ice

            IF ( REMOV_ICE_SO2 .LE. CGRID( COL, ROW, LAY, 52 ) ) THEN
              REMOV_ICE_SO2 = REMOV_ICE_SO2
            ELSE
              REMOV_ICE_SO2 = CGRID( COL, ROW, LAY, 52 )
                    END IF

            ADS_SO2_RATIO = ( REMOV_ICE_SO2 ) / ( CGRID( COL, ROW, LAY, 52 ) )

            ADS_ICE_SO2 = ( ( REMOV_ICE_SO2 * ( ( PRES ( COL, ROW, LAY ) ) / ( UNIVERR * TA( COL, ROW, LAY ) ) ) )
/ 1000 )                                                    ! convert to moles/L or M

          END IF

                END DO
```

```
C… Solve for reaction rate constant
                kH2SO4 = ( ( 7.2e7 ) * ( EXP( -4000 / TA( COL, ROW, LAY ) ) ) )          ! rate constant for SO2 and H2O2 reaction
(M-2 S-1) (Ervens et al. 2004)

          SPC = 0
          DO SPC = 1, NSPCSD

            IF (SPC .EQ. 13) THEN                                                                    ! SPC 13 = H2O2
              REACT_H2O2 = kH2SO4 * TAUCLD * ADS_ICE_SO2 * ADS_ICE_H2O2 * HPLUSCONC
!amount of H2O2 reacting with SO2 in moles/L or M
              DELH2O2 = ( ( REACT_H2O2 * 1000 * ( UNIVERR * TA( COL, ROW, LAY ) ) ) / ( PRES ( COL, ROW, LAY ) ) )
!amount of H2O2 reacting with SO2 in mixing ratio
               IF ( DELH2O2 .LE. CGRID( COL, ROW, LAY, 13 ) ) THEN
                 DELH2O2 = DELH2O2
               ELSE
                  DELH2O2 = CGRID( COL, ROW, LAY, 13 )
               END IF

               CGRID( COL, ROW, LAY, 13 ) = CGRID( COL, ROW, LAY, 13 ) - DELH2O2              ! new ending conc for H2O2
            END IF

            IF (SPC .EQ. 52) THEN                                                                ! SPC 52 = SO2
              REACT_SO2 = kH2SO4 * TAUCLD * ADS_ICE_SO2 * ADS_ICE_H2O2 * HPLUSCONC
!amount of SO2 reacting with H2O2 in moles/L or M
              DELSO2 = ( ( REACT_SO2 * 1000 * ( UNIVERR * TA( COL, ROW, LAY ) ) ) / ( PRES ( COL, ROW, LAY ) ) )
!amount of SO2 reacting with H2O2 in mixing ratio

              IF ( DELSO2 .LE. CGRID( COL, ROW, LAY, 52 ) ) THEN
                 DELSO2 = DELSO2
              ELSE
                 DELSO2 = CGRID( COL, ROW, LAY, 52 )
```

```
              END IF
              CGRID( COL, ROW, LAY, 52 ) = CGRID( COL, ROW, LAY, 52 ) - DELSO2                    ! new ending conc for SO2
            END IF

C... Determine amount of sulfate that formed
            IF (SPC .EQ. 74) THEN                                                                ! SPC 74 = accumulation mode sulfate
              REACT_H2SO4 = kH2SO4 * TAUCLD * ADS_ICE_SO2 * ADS_ICE_H2O2 * HPLUSCONC
! amount of sulfate formed
              DELH2SO4 = ( ( REACT_H2SO4 * 1000 * ( UNIVERR * TA( COL, ROW, LAY ) ) ) / ( PRES ( COL, ROW, LAY ) ) )
! amount of sulfate formed in correct units
             CGRID( COL, ROW, LAY, 74 ) = CGRID( COL, ROW, LAY, 74 ) + ( DELH2SO4 )          ! new ending conc for ASO4J

            END IF

          END DO

         END IF

       END DO
     END DO
   END DO

C...Ice Code is finished
```

References

Abbatt, J. P.D.: Interaction of HNO3 with water-ice surfaces at temperatures of the free troposphere, Geophys. Res. Lett., **24**, 1479–1482, 1997.

Allen, D. J., Pickering, K. E., Pinder, R. W., Henderson, B. H., Appel, K. W., and Prados, A.: Impact of lightning-NO on eastern United States photochemistry during the summer of 2006 as determined using the CMAQ model, *Atmos. Chem. Phys.*, **12**, 1737-1758, doi:10.5194/acp-12-1737-2012, 2012.

Appel, K., W., *Examination of the 2002 – 2006 CMAQ simulations: reviewing model performance over a five-year period*. EPA. April 7, 2010.

Appel, K. W., Foley, K. M., Bash, J. O., Pinder, R. W., Dennis, R. L., Allen, D. J., and Pickering, K.: A multi-resolution assessment of the Community Multiscale Air Quality (CMAQ) model v4.7 wet deposition estimates for 2002–2006, *Geosci. Model Dev.*, **4**, 357-371, doi:10.5194/gmd-4-357-2011, 2011.

Boccippio, D., Cummings, K., Christian, H., and Goodman, S.: Combined satellite- and surface-based estimation of the intracloud-cloud-to-ground lightning ratio over the continental United States, Mon. Weather. Rev., **129**, 108–122, 2001.

Carver, G., Barjat, H., and Cox, R. A.: "Datasheets for Heterogeneous Reactions on Ice." *IUPAC: Subcommittee for Gas Kinetic Data Evaluation*. Centre for Atmospheric Science, 1999. Web. 24 Aug. 2012. <http://www.iupac-kinetic.ch.cam.ac.uk/>.

Chu, L., Diao G., and Chu, L. T.: Heterogeneous interaction of SO2 on H2O2-ice films at 190–210 K, J. Phys. Chem. A., **104**, 7565–7573, 2000.

Civerolo, K., Hogrefe, C., Zalewsky, E., Hao, W., Sistla, G., Lynn, B., Rosenzweig, C., Kinney, P. L.: Evaluation of an 18-year CMAQ simulation: Seasonal variations and long-term temporal changes in sulfate and nitrate. *Atmos. Environ*., **44**, 3745–3752, 2010.

Clegg, S. M., and Abbatt, J. P. D.: Uptake of gas-phase SO_2 and H_2O_2 by ice surfaces: Dependence on partial pressure, temperature, and surface acidity, *J. Phys. Chem. A*, **105**, 6630 –6636, 2001a.

Clegg, S. M., and Abbatt, J. P. D.: Oxidation of SO_2 by H_2O_2 on ice surfaces at 228 K: a sink for SO_2 in ice clouds, *Atmos. Chem. Phys*., **1**, 73-78, doi:10.5194/acp-1-73-2001, 2001b.

Conklin, M. H., Sommerfeld, R. A., Laird S. K., and Villinski, J. E.: Sulfur dioxide reactions on ice surfaces: Implications for dry deposition to snow, Atmos. Environ., **27A**, 159–166, 1993.

Ervens, B., Feingold, G., Frost, G. J., and Kreidenweis, S. M.: A modeling study of aqueous production of dicarboxylic acids: 1. Chemical pathways and speciated organic mass production, *J. Geophys. Res.*, **109**, D15205, doi:10.1029/2003JD004387, 2004.

Finlayson-Pitts, B. J. and Pitts, J. N.: *Chemistry of the Upper and Lower Atmosphere*. Academic Press, San Diego, 2000.

Henderson, B. H., Pinder, R. W., Crooks, J., Cohen, R. C., Hutzell, W. T., Sarwar, G., Goliff, W. S., Stockwell, W. R., Fahr, A., Mathur, R., Carlton, A. G., and Vizuete, W.: Evaluation of simulated photochemical partitioning of oxidized nitrogen in the upper troposphere, Atmos. Chem. Phys., **11**, 275–291, doi:10.5194/acp-11-275-2011, 2011.

Ivanova, D. D., Mitchell, L., Arnott, W.P., and Poellot, M., A GCM parameterization for bimodal size spectra and ice mass removal rates in mid-latitude cirrus clouds, Atmos. Res., **59**, 89– 113, 2001.

Jacob, D. J.: *Introduction to Atmospheric Chemistry*. Princeton University Press, Princeton, 1999.

Krämer, M., Schiller, C., Voigt, C., Schlager, H., and Popp, P. J.: A climatological view of HNO3 partitioning in cirrus clouds, Q. J. Roy. Meteor. Soc., **134**, 905–912, doi:10.1002/qj.253, 2008.

Marécal, V., Pirre, M., Rivière, E. D., Pouvesle, N., Crowley, J. N., Freitas, S. R., and Longo, K. M.: Modelling the reversible uptake of chemical species in the gas phase by ice particles formed in a convective cloud, *Atmos. Chem. Phys.*, **10**, 4977-5000, doi:10.5194/acp-10-4977-2010, 2010.

Mather, J. H., McFarlane, S. A., Miller, M. A., and Johnson K. L.: Cloud properties and associated radiative heating rates in the tropical western Pacific, *J. Geophys. Res.*, **112**, D05201, doi:10.1029/2006JD007555, 2007.

Mitra, S. K., Barth, S., and Pruppacher, H. R.: A laboratory study of the scavenging of SO2 by snow crystals, Atmos. Environ., **24A**, 2307–2312, 1990.

Popp, P. J., Gao, R. S., Marcy, T. P., Fahey, D. W., Hudson, P. K., Thompson, T. L., K¨archer, B., Ridley, B. A., Weinheimer, A. J., Knapp, D. J., Montzka, D. D., Baumgardner, D., Garrett, T. J., Weinstock, E. M., Smith, J. B., Sayres, D. S., Pittman, J. V., Dhaniyala, S., Bui, T. P., and Mahoney, M. J.: Nitric acid uptake on subtropical cirrus cloud particles, J. Geophys. Res., **109**, D06302, doi:10.1029/2003JD004255, 2004.

Pouvesle, N., Kippenberger, M., Schuster G., and Crowley, J. N.: The interaction of H_2O_2 with ice surfaces between 203 and 233 K. *Phys. Chem. Chem. Phys.*, **12**, 15544-15550, doi: 10.1039/C0CP01656J, 2010.

Rogers, R. R., and Yau, M. K.: *A Short Course in Cloud Physics*. Pergamon Pr., Oxford, 1989.

Seinfeld, J. H., and Pandis, S. N.: *Atmospheric Chemistry and Physics: From Air Pollution to Climate Change*. Wiley, Hoboken, 2006.

Tabazadeh, A., Toon, O. B., and Jensen, E. J.: A surface chemistry model for nonreactive trace gas adsorption on ice: Implications for nitric acid scavenging by cirrus, Geophys. Res. Lett., **26(14)**, 2211–2214, 1999.

"Unisys Weather." *Unisys Weather*. 2005: Web. 12 Sept. 2012. <http://weather.unisys.com/>.

Wallace, J. M., and Hobbs, P. V.: *Atmospheric Science: An Introductory Survey*. Elsevier, Amsterdam, 2006.